April 2020

On Characterizing Quantum Processes and Detectors

Kevin Valson Jacob
Louisiana State University and Agricultural and Mechanical College

ON CHARACTERIZING QUANTUM PROCESSES AND DETECTORS

A Dissertation

Submitted to the Graduate Faculty of the
Louisiana State University and
Agricultural and Mechanical College
in partial fulfillment of the
requirements for the degree of
Doctor of Philosophy

in

The Department of Physics and Astronomy

by
Kevin Valson Jacob
M.Sc., Indian Institute of Technology Kanpur, 2015
May 2020

To my wife Anu

Many women do noble things,

but you surpass them all.

Acknowledgments

First of all, I thank God for enabling me to produce this scholarly work.

I thank Prof. Jonathan P. Dowling for advising my thesis. His belief in my ability to do research has boosted my confidence in my ability to be a professional scientist.

I thank Prof. Mark Wilde for teaching me various aspects of quantum information such as quantum computing, quantum information theory, and gaussian quantum information. I thank Dr. Omar Magana-Loaiza for stimulating discussions, and also for serving on my dissertaion committee. I thank Prof. A.R.P. Rau for teaching me advanced quantum mechanics, group theory, and mathematical methods. He has taught me by example how to be a good teacher of physics. I thank Prof. Rongying Jin and Prof. Louis Haber for serving on my dissertation committee.

I thank Prof. Masahiro Takeoka for providing me an opportunity to carry out collaborative research in Japan during the summer of 2019.

I thank my collaborators Anthony Mirasola, Sushovit Adhikari, Rajveer Nehra, Wojciech Roga, and Pratik Barge.

I thank Prof. S.S. Manoharan, Prof. Joseph John and Prof. Chacko Jacob for inspiring me to pursue a Ph.D. I thank Abel Juhan Thomas, my dearest friend, for his friendship and trust. I thank Dr. Kevin McKee for his insights on life which have often helped me during the course of my graduate studies. I thank my friends at the quantum science and technology group for their help and support during my graduate studies.

I thank my parents for their countless sacrifices in enabling me to pursue my interests. Their love, support, and encouragement was of immense value in molding me into who I am today .

Most importantly, I thank my wife Anu for being there for me whenever I needed her. Her constant support and belief in me as well as her companionship enabled this dissertation.

Table of Contents

List of Figures

Abstract

In 2009, physicists at the National Institute of Standards and Technology in Colorado, Boulder developed what could arguable be called the first rudimentary quantum computer [1]. The past decade has seen unprecedented improvements in quantum information science culminating in the demonstration of quantum supremacy — that quantum computers can solve problems that are impractical to be solved on the best supercomputers [2]. This remarkable progress necessitates the development of techniques to characterize the quantum devices that are being developed. In my thesis, I will focus on such devices that manipulate and detect light.

In Chapter 1, I will introduce the reader to the historical underpinnings of the study of light. After surveying the history of light since time immemorial, I will delve into the developments in the study of light in the 19^{th} and the early 20^{th} century. I will then present a brief introduction to quantum mechanics. I end this chapter by demonstrating how light is quantized.

In Chapter 2, I will introduce the various tools necessary to delve into this dissertation. After defining quadrature operators and Wigner functions, I will introduce various states of light used in this thesis. I will then discuss how the evolution, as well as detection of quantum optical states, are modelled. I will then present the formalism of Gaussian quantum information that simplifies the manipulation of certain states of light. Finally, I will briefly talk about quantum metrology and show its advantage in phase estimation.

In Chapter 3, I will introduce a method to characterize linear and quadratically nonlinear optical systems. After motivating the need for this work, I will introduce the modifications necessary to the standard Mach-Zehnder interferometer in order to characterize optical systems with it. I will then show how to characterize linear optical systems with coherent probes. I will also show that this scheme is shot-noise limited. I will then show that by using single photons in addition, we can characterize quadratically nonlinear optical systems. Finally, I will show that no advantage is gained in sensitivity by using squeezed

light along with coherent light as probes.

In Chapter 4, I will introduce a method to characterize photodetectors. This is done by developing an experimental method to find the Wigner functions of the POVM set corresponding to a photodetector. After motivating the necessity of this work as well as describing the proposed experimental setup, I will show how this scheme can be used to characterize a photon-number-resolving detector. I will then show that if we have some prior knowledge of the detector then it can drastically reduce the resource requirement of characterizing the detector. Finally, I will make the characterization robust against experimental noise by using tools from convex quadratic optimization.

At last, I summarize my conclusions in Chapter 5.

Chapter 1
Introduction

It is the function of science to discover the existence of a general reign of order in nature and to find the causes governing this order.

— Dmitri Mendeleev

The Principles of Chemistry

1.1 A brief introduction to science

Humanity has always displayed a curiosity to understand the natural world around it. One of the early sciences amenable to the discovery of humans was astronomy, where astronomers of ancient civilizations observed stars and planets in the night sky. They noticed patterns among stars such as constellations, which resembled familiar objects such as a hunter (Orion) or a bear (Ursa Major). They observed the waxing and the waning of the moon as well as eclipses, and came up with mathematical models to predict them.

Modern science is an endeavor which spans across various scales of space and time: from the smallest subatomic particles to the vast cosmos and all within it, from the simplest of molecules to engineered materials and drugs, from the tiniest viruses to human physiology, from the simplest engines to nuclear weaponry, from nanorobots to massive space shuttles, from the early universe to its inevitable end. What distinguishes modern science from ancient protosciences is the existence of criteria which can validate or falsify proposed theories.

This emphasis on truth in modern science not only allowed us to develop accurate theories but also to develop new theories using pre-existing theories as its building blocks. In the modern world, the availability of such widely tested pre-existing theories allows scientists to develop ground-breaking science without developing all of its ingredients from scratch. For example, a scientist can study the early universe without rederiving quantum mechanics and general relativity. Not only this, the availability of well-tested theories allows

scientists to break down new problems that they pursue into various components, each of which can be solved by specialists. This allows various collaborative scientific research, producing new science which could not have been produced by a single scientist alone.

These distinguishing characters of modern science are among the primary reasons for the technological revolution around us. Humans have learned to adapt scientific theories to their advantage resulting in tremendous developments in the field of computation, communication, construction, agriculture, chemical synthesis, transportation, manufacturing, clothing, and even entertainment. These developments along with trade, commerce, and a sophisticated system of markets have led to drastic improvements in the human condition.

In this thesis, I will turn my attention to a part of the technological revolution - how our understanding of light has paved a way to manipulate it to our advantage. In particular, I will focus on one part of that puzzle: How do we characterize devices that manipulate light? The resulting technologies from the manipulation of light promise us advantages in computation, sensing, and communication.

1.2 What is light?

> All the fifty years of conscious brooding have brought me no closer to answer the question, 'What are light quanta?'. Of course, today every rascal thinks he knows the answer, but he is deluding himself.
>
> — Albert Einstein
>
> Letter to Michael Besso

Visible light is demonstrably different from the matter that we see around us. This piqued the curiosity of humans to enquire into the nature of light since antiquity [3]. Ancient Egyptians believed that light is the ocular fire from the eyes of the sun god Ra. In contrast, in 4^{th} century BCE, Plato taught that light consists of rays emitted by eyes. Around the same time, the ancient Chinese text *Mozi* was written which contains the earliest known description of the pinhole camera.

Around 300 BCE, Euclid in *Optica* demonstrated that light travels in straight lines by

studying the reflection of light. In the second century CE, Ptolemy studied refraction — the way light bends in certain transparent materials such as water or glass, and developed a small-angle approximation to the law of refraction.

In the 11^{th} century, Ibn Al-Haytham – an Arab scientist extensively studied light. He thoroughly studied the pinhole camera and described the camera obscura effect. He split light into its constituent colors, and magnified objects with lenses. He posited that light doesn't travel instantaneously, and that the refraction of light was due to light travelling at different velocities in different media.

In the 16^{th} century, the German astronomer Johannes Kepler developed a system of laws of planetary motion. He noted that the human eye also posesses an aperture and therefore should be treated in the same way as a pinhole camera.

In the early 17^{th} century, Galileo invented a telescope capable of examining various heavenly bodies. He examined in detail the craters of the moon, discovered four satellites of Jupiter, observed sunspots, and observed a supernova. His discoveries were pivotal in the confirmation of the heliocentric model of the solar system.

In early 17^{th} century, Descartes used a tennis ball analogy to derive the laws of reflection and refraction. Further, Descartes postulated that light propagates as waves in a medium called *plenum* which is present everywhere and is capable of supporting light waves. This is similar to waves of water that one observes on a beach. Along with Descartes, Pierre de Fermat rederived the laws of refraction using the principle of least time.

In late 17^{th} century, Christiaan Huygens developed a wave theory of light where he postulated that at each moment each point of an advancing wavefront emanates secondary waves; and the wavefront at a later time can be found as the tangent surface to these secondary waves. According to Huygens, light consisted of longitudinal waves as opposed to the transverse nature of light, which was discovered later.

In contrast to the wave theory of light, in the late 17^{th} century, Sir Isaac Newton — one of the greatest scientists to have ever lived — postulated that light is made of particles

which he named corpuscles. To be consistent with this postulate, Newton hypothesized that light travels faster in transparent media than in the atmosphere — a hypothesis later proven to be false. This schism between the supporters of the wave nature and the particle nature of light continued for centuries. Newton also used prisms to split white light into various colors and recombine them, thereby demonstrating that color is a property of light. Newton also developed the first reflecting telescope. In contrast to telescopes using refraction, reflecting telescopes suffer less from chromatic abberation.

In the early 19^{th} century, Thomas Young proposed a double slit experiment, wherein light from a source was allowed to pass through two slits. The resulting pattern of fringes, with crests and troughs, could no longer simply be explained using the corpuscular theory. Further, Young used his experiment to relate the wavelength of light to its color.

Further confirmations of the wave theory came around the same time when Fresnel developed a theory of diffraction: a theory which explains how light bends around objects under the assumption that it was a wave. This theory predicted that the shadow of a disk illuminated with a point source of light will have a bright spot at its center. This counter-intuitive hypothesis, when confirmed by experiments, led to the widespread acceptance of the wave theory of light. Fresnel and Arago also inquired into the polarization of light. He was able to obtain circularly polarized light, the properties of which could only be explained by assuming that light is a transverse wave.

Notable insights into the wave nature of light were made in the latter part of the 19^{th} century by James Clerk Maxwell, who discerned the governing equations of light as a transverse electromagnetic wave. Not only did this reproduce the known value of the speed of light, this unified the two forces of nature known at that time - electricity and magnetism. This description of light as an electromagnetic wave was demonstrated by Heinrich Hertz in 1888.

In the 1880s, Michelson and Morley disproved the existence of any substance through which the electromagnetic waves propagate. They did this by using a Michelson interfer-

ometer. They expected to see a shift in the pattern of fringes due to the earth's motion with respect to ether. However, the null result of this experiment disproved the existence of ether. Further, it showed that the speed of light is the same in all reference frames.

1.3 Light in the twentieth century

That the constancy of the speed of light for all inertial observers had manifest consequences was only discovered in the twentieth century by Albert Einstein. Working from a patent office in Germany, in 1905 Einstein developed the special theory of relativity assuming only two postulates: that the laws of physics are the same for all inertial observers, and that the speed of light is the same for all observers. Based on these, Einstein derived a set of coordinate transformations between reference frames referred to as Lorentz transformations. Using these, he was able to explain phenomenon such as length contraction and time dilation.

Besides the special theory of relativity, Einstein also developed the general theory of relativity which provides a geometric understanding of space-time. This theory was founded on the equivalence principle — that being in an accelerated reference frame and being in a gravitational field were physically identical. Einstein used this theory to correctly solve the problem of the precession of the perihelion of mercury. One of the more dramatic predictions of the general theory of relativity was the manner in which light bends around a massive object. Einstein predicted that light from the sun bends by about 1.83 arc seconds — about double the value predicted by Newtonian mechanics. With the confirmation of this prediction by Sir Arthur Eddington in 1919, Einstein's theory became widely accepted. Further confirmations of the theory include the observation of gravitational redshift of light and the recent observation of gravitational waves.

It was the work of Albert Einstein that brought the particle theory of light came back into prominence. In order to explain the photoelectric effect of metals emitting electrons when ultraviolet radiation was incident on it, Einstein posited that ultraviolet light comes in packets referred to as quanta. These quanta were discrete chunks of energy, unlike the

corpuscular theory of Newton, which described light as particles localized in space and time.

A complete resolution of the wave-particle duality of light did not come until the birth of quantum mechanics, which posited that quantum states of light exhibit both wave-like and particle-like properties.

1.4 Quantum mechanics

> I think I can safely say that no one understands quantum mechanics.
>
> — Richard P. Feynman
>
> The Messenger Lectures

Around 1925, a new way of understanding the world arose through the works of Max Born, Werner Heisenberg, Pascual Jordan, Paul Dirac, and Erwin Schrödinger. This revolutionary theory known as quantum mechanics posited the principle of complementarity wherein two observables are so related that the precise knowledge of one leads to a complete uncertainty in the other. This leads to the well-known uncertainty principle.

In 1927, Paul Dirac applied quantum theory to light where he proposed that each mode of the electromagnetic field is a quantized simple harmonic oscillator. A single excitation of a particular mode would give rise to a photon. In this case, the uncertainty relation leads to an uncertainty between the electric and the magnetic fields of the electromagnetic wave. We will discuss the quantization of light in detail in Sec. 1.5.

In the modern formulation of the theory of quantum mechanics, a pure state of light is completely described by a vector $|\Psi\rangle$ in an infinite dimensional Hilbert space. More generally, a mixed state of light is described by a density matrix ρ. The action of the Hamiltonian on this state can be represented in two equivalent ways: via the Schrodinger picture where the state evolves in time, or via the Heisenberg picture where all operators corresponding to the state evolve in time. In Schrodinger picture, this evolution is given by the Schrodinger equation as

$$i\hbar\frac{\partial|\Psi\rangle}{\partial t} = \hat{H}|\Psi\rangle \tag{1.1}$$

$$i\hbar\frac{\partial\hat{\rho}}{\partial t} = \left[\hat{H}, \hat{\rho}\right] \tag{1.2}$$

In contrast, in Heisenberg picture, the operators corresponding to the state evolve as

$$i\hbar\frac{\partial\hat{O}}{\partial t} = \left[\hat{O}, \hat{H}\right] \tag{1.3}$$

Although completely equivalent in their predictions, these picture are not equivalent in their computational complexity [4].

1.5 Quantization of light

In this section we will see how light is quantized. We will draw an analogy between the electromagnetic field and a simple harmonic oscillator. We will see that the photon is an elementary excitation of a normal mode of the electromagnetic field. This will in turn help us understand and identify quantum states of light and their properties. This section closely follows the discussion in Chapter 2 of Ref. [5].

We will begin by stating the Maxwell equations in vacuum in the absence of currents or charges. In SI units, these are given as:

$$\nabla \cdot \boldsymbol{E} = 0, \tag{1.4}$$

$$\nabla \cdot \boldsymbol{B} = 0, \tag{1.5}$$

$$\nabla \times \boldsymbol{E} = -\frac{\partial \boldsymbol{B}}{\partial t}, \tag{1.6}$$

$$\nabla \times \boldsymbol{B} = \frac{1}{c^2}\frac{\partial \boldsymbol{E}}{\partial t}, \tag{1.7}$$

where $\boldsymbol{E}$ and $\boldsymbol{B}$ are the electric and magnetic fields respectively, and c is the speed of light in vacuum. We will restrict our attention to a one dimensional cavity along the z-direction with perfectly conducting walls at $z = 0$ and $z = L$. We will assume that the light is polarized along x-axis i.e

$$\boldsymbol{E}(\boldsymbol{r}, t) = E_x(z, t)\hat{x}, \tag{1.8}$$

where $\hat{x}$ is a unit polarization vector. A single mode field obeying the Maxwell equations and boundary conditions is given as

$$E_x(z,t) = \left(\frac{2\omega^2}{V\epsilon_0}\right)^{\frac{1}{2}} q(t)\sin(kz), \tag{1.9}$$

where V is the effective volume of the cavity, ϵ_0 the permittivity of free space, ω the frequency of the mode, k its wavenumber, and the linear dispersion relation in vacuum is

$$\omega = ck. \tag{1.10}$$

Further, the perfectly conducting walls imposes the additional constraint that the field vanishes at the boundaries of the cavity. This implies

$$k = \frac{m\pi}{L}, \;\; m \in \mathbb{Z}^+. \tag{1.11}$$

Note from Eq.(1.9) that $q(t)$ has the dimensions of distance. Indeed, we shall see that it shall act as the canonical position. Having found an expression for the electric field in the cavity, we can substitute it into the Maxwell equations so as to obtain an expression for the magnetic field as

$$\boldsymbol{B}(\boldsymbol{r},t) = B_y(z,t)\hat{y}, \tag{1.12}$$

where

$$B_y(z,t) = \frac{c}{k}\left(\frac{2\omega^2}{V\epsilon_0}\right)^{\frac{1}{2}} \dot{q}(t)\cos(kz), \tag{1.13}$$

where $\dot{q}(t)$ shall act as the canonical momentum. We can then write the classical field energy of the single mode field i.e. the Hamiltonian as

$$H = \frac{1}{2}\int dV \left[\epsilon_0 \boldsymbol{E}^2(\boldsymbol{r},t) + \frac{1}{\mu_0}\boldsymbol{B}^2(\boldsymbol{r},t)\right], \tag{1.14}$$

$$= \frac{1}{2}\int dV \left[\epsilon_0 E_x^2(z,t) + \frac{1}{\mu_0}B_y^2(z,t)\right], \tag{1.15}$$

where μ_0 is the permeability of free space. Substituting Eq.(1.9) and Eq.(1.13) in Eq.(1.15), and using the fact that $\dot{q}(t) \equiv p(t)$ and that $c^2 = (\epsilon_0 \mu_0)^{-1}$, we obtain

$$H = \frac{1}{V} \int dV \left[\omega^2 q^2(t) \sin^2(kz) + p^2(t) \cos^2(kz) \right] \tag{1.16}$$

$$= \frac{1}{V} \int dV \left[\omega^2 q^2(t) \left(\frac{1 - \cos(2kz)}{2} \right) + p^2(t) \left(\frac{1 + \cos(2kz)}{2} \right) \right]. \tag{1.17}$$

Due to the periodic boundary conditions, the sinusoidal terms in the integral vanish, and we are left with

$$H = \frac{1}{2}(p^2 + \omega^2 q^2) \tag{1.18}$$

This is the Hamiltonian of a simple harmonic oscillator. In order to quantize this Hamiltonian, we follow the canonical quantization procedure and replace the canonical variable q and p with their operator equivalents $\hat{q}$ and $\hat{p}$. We now impose the canonical commutation relation between $\hat{q}$ and $\hat{p}$ as

$$[\hat{q}, \hat{p}] = i\hbar \mathbb{1}. \tag{1.19}$$

Further insights about this Hamiltonian can be obtained by defining the ladder operators as linear combinations of the canonical position and momentum operators as

$$\hat{a} = \frac{\omega \hat{q} + i\hat{p}}{\sqrt{2\hbar\omega}}, \tag{1.20}$$

$$\hat{a}^\dagger = \frac{\omega \hat{q} - i\hat{p}}{\sqrt{2\hbar\omega}}. \tag{1.21}$$

From Eq. (1.19), we observe that the annihilation operator $\hat{a}$ and the creation operator $\hat{a}^\dagger$ satisfy the commutation relation

$$[\hat{a}, \hat{a}^\dagger] = \mathbb{1}. \tag{1.22}$$

Finally, we can use Eq.(1.18) to write the Hamiltonian operator as

$$\hat{H} = \frac{\hbar\omega}{2}(2\hat{a}^\dagger \hat{a} + 1) \tag{1.23}$$

This is the Hamiltonian of a single-mode of the electromagnetic field. An elementary excitation of this field gives us a photon.

Chapter 2
Elements of Quantum Optics

Having quantized the electromagnetic field, in this chapter I will provide a mathematical description of the elements of quantum optics, namely quantum states of light, and devices that evolve and detect the states of light. In order to do that, I will first define a few tools which will allow us to describe these elements. Understanding the various properties of these elements will help us manipulate light to our advantage. I will also introduce Gaussian quantum information and quantum metrology.

2.1 Tools of the trade

In this section, I will introduce two tools that will be of great use throughout this thesis. I will first introduce quadrature operators, and then define Wigner functions — a useful tool to visualize quantum states of light.

2.1.1 Quadrature operators

An insightful tool to understand quantum states of light is via quadrature operators. We define them as

$$\hat{X}_1 \equiv \frac{\hat{a} + \hat{a}^\dagger}{2}, \tag{2.1}$$

$$\hat{X}_2 \equiv \frac{\hat{a} - \hat{a}^\dagger}{2i}. \tag{2.2}$$

Note that alternate definitions of the quadrature operators exist, which differ from this definition by a constant factor. From Eqs. (1.20) and (1.21), we see that quadrature operators are the dimensionless versions of the position and momentum operators of the electromagnetic field. From Eq. (1.22), it can be easily verified that the quadrature operators satisfy the commutation relation

$$[\hat{X}_1, \hat{X}_2] = \frac{i\mathbb{1}}{2}. \tag{2.3}$$

Further, these operators satisfy the uncertainty relation

$$\langle(\Delta\hat{X}_1)^2\rangle\langle(\Delta\hat{X}_2)^2\rangle \geq \frac{1}{16}, \tag{2.4}$$

where the variance of the quadrature operators is given as

$$\langle(\Delta\hat{X}_i)^2\rangle \equiv \langle\hat{X}_i{}^2\rangle - \langle\hat{X}_i\rangle^2, \;\; i = 1, 2, \tag{2.5}$$

and the expectation value is evaluated for any quantum state.

2.1.2 Wigner quasi-probability distributions

A useful tool to visualize quantum states of light is the Wigner quasi-probability distribution [6]. The prefix 'quasi' is intended to signify that the Wigner distribution doesn't satisfy the non-negativity requirement of classical probability distributions. In particular, if the Wigner function corresponding to a state attains negative values, then the state exhibits quantumness [7].

For an arbitrary state $\hat{\rho}$, this distribution is defined as

$$W(q,p) \equiv \frac{1}{2\pi\hbar}\int_{-\infty}^{\infty}\left\langle q+\frac{x}{2}\middle|\hat{\rho}\middle|q-\frac{x}{2}\right\rangle \exp\left(\frac{ipx}{\hbar}\right)dx, \tag{2.6}$$

where $\left|q \pm \frac{x}{2}\right\rangle$ are eigenstates of the position operator. An alternate definition of the Wigner distribution is

$$W(\alpha) = \frac{1}{\pi^2}\int \exp(\lambda^*\alpha - \lambda\alpha^*)\mathrm{Tr}\left[\hat{\rho}\hat{\mathcal{D}}(\lambda)\right]\, d^2\lambda, \tag{2.7}$$

where $\alpha = q + ip$, and $\hat{\mathcal{D}}(\lambda)$ is the displacement operator defined as:

$$\hat{\mathcal{D}}(\alpha) = \exp\left\{\alpha\hat{a}^\dagger - \alpha^*\hat{a}\right\}. \tag{2.8}$$

Finally, a useful representation of the Wigner function operator is given as [5]

$$\hat{W}(\alpha) = \frac{2}{\pi}\sum_{n=0}^{\infty}(-1)^n\hat{\mathcal{D}}(\alpha)|n\rangle\langle n|\hat{\mathcal{D}}^\dagger(\alpha). \tag{2.9}$$

In order to evaluate the Wigner function of a state ρ, we can use the Born rule as

$$W(\alpha) = \mathrm{Tr}[\hat{\rho}\hat{W}(\alpha)] \tag{2.10}$$

When the Wigner function of a state of light has a gaussian form, it is called a gaussian state. Gaussian states are important in quantum optics and quantum information as they have many properties which make them amenable to mathematical manipulation. In particular, a gaussian state is fully characterized by the first and the second moments of the quadrature operators of the state.

2.2 Quantum states of light

In this section, I will introduce some of the states of the electromagnetic field that are of relevance to this thesis. I will first introduce Fock states. I will then discuss coherent states, squeezed states, and thermal states.

2.2.1 Fock states

The Hamiltonian of the electromagnetic field was defined in Eq. (1.23), and resembles that of a quantum harmonic oscillator. Akin to a quantum harmonic oscillator, this Hamiltonian has a discrete spectrum with equally spaced consecutive levels. The form of this Hamiltonian leads us to define the number operator as

$$\hat{N} = \hat{a}^\dagger\hat{a}. \tag{2.11}$$

It can be easily observed that the number operator commutes with the Hamiltonian, and therefore has simultaneous eigenstates. The ground state of this Hamiltonian is referred to as the vacuum state, denoted by $|0\rangle$. It is the state of the electromagnetic field with no

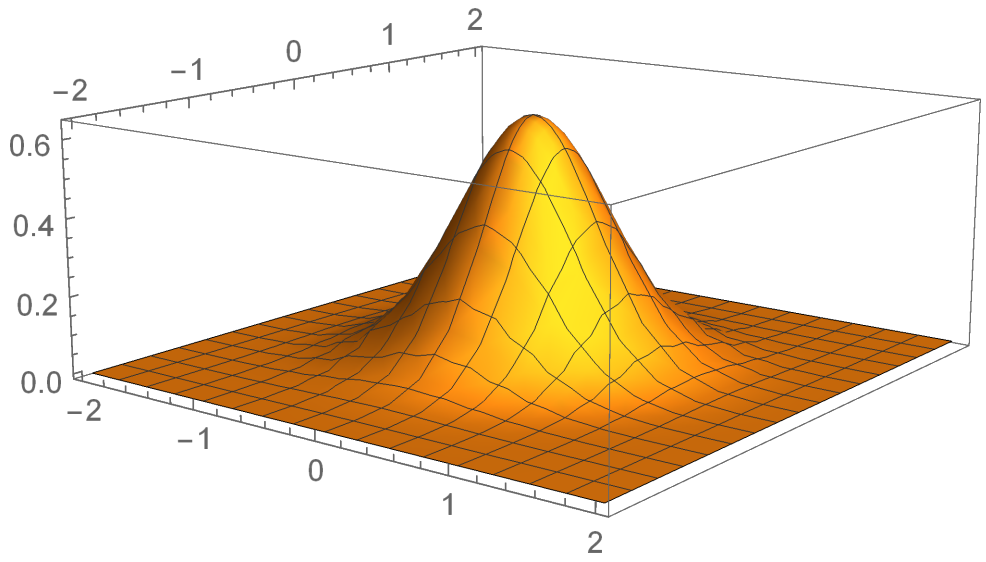

Figure 2.1: Wigner function of a vacuum state. The distribution is Gaussian centered around the origin.

excitations i.e. $\langle \hat{N} \rangle_{|0\rangle} = 0$. Although there are no excitations, the electric and magnetic fields corresponding to this state are fluctuating. In fact, such fluctuations of the vacuum state saturates the uncertainty relation as given in Eq. (2.4). The Wigner function of a vacuum state is shown in Fig. 2.1.

Higher excitations of the electromagnetic field are referred to as Fock states or number states, where the n^{th} excitation is denoted by $|n\rangle$. The action of creation and annihilation operators on Fock states are given as

$$\hat{a}|n\rangle = \sqrt{n}|n-1\rangle, \tag{2.12}$$

$$\hat{a}^\dagger|n\rangle = \sqrt{n+1}|n+1\rangle. \tag{2.13}$$

Furthermore, the Fock state $|n\rangle$ can be obtained from the vacuum state $|0\rangle$ by successively operating the creation operator as:

$$|n\rangle = \frac{(\hat{a}^\dagger)^n}{\sqrt{n!}}|0\rangle. \tag{2.14}$$

The expectation value of the quadrature operators vanish for these states, i.e.,

$$\langle n|\hat{X}_1|n\rangle = 0, \tag{2.15}$$

$$\langle n|\hat{X}_2|n\rangle = 0. \tag{2.16}$$

However, the uncertainties of the quadrature operators don't vanish. For the Fock state, $|n\rangle$, they are

$$\langle(\Delta\hat{X}_{1,2})^2\rangle = \frac{2n+1}{4}. \tag{2.17}$$

Fock states are orthonormal to each other. That is for two Fock states,

$$\langle m|n\rangle = \delta_{m,n}, \tag{2.18}$$

where $\delta_{m,n}$ is the Kronecker delta. Fock states also form a complete basis since the identity operator can be resolved in terms of the Fock states as:

$$\sum_{n=0}^{\infty} |n\rangle\langle n| = \mathbb{1}. \tag{2.19}$$

This implies that any quantum optical state can be expressed as a linear combination of Fock states. As mentioned earlier, the Fock states have definite energy, which is given as

$$E_{|n\rangle} = \hbar\omega\left(n + \frac{1}{2}\right). \tag{2.20}$$

The Wigner function corresponding to a Fock state $|n\rangle$ is given as

$$W(\alpha) = \frac{2}{\pi}(-1)^n\mathcal{L}_n(4|\alpha|^2)\exp\big(-2|\alpha|^2\big), \tag{2.21}$$

where $\mathcal{L}_n(\zeta)$ is the n^{th} Laguerre polynomial. Except for the vacuum state, Fock states are not Gaussian. In Fig. 2.2, the Wigner function corresponding to the Fock state $|1\rangle$ is

plotted.

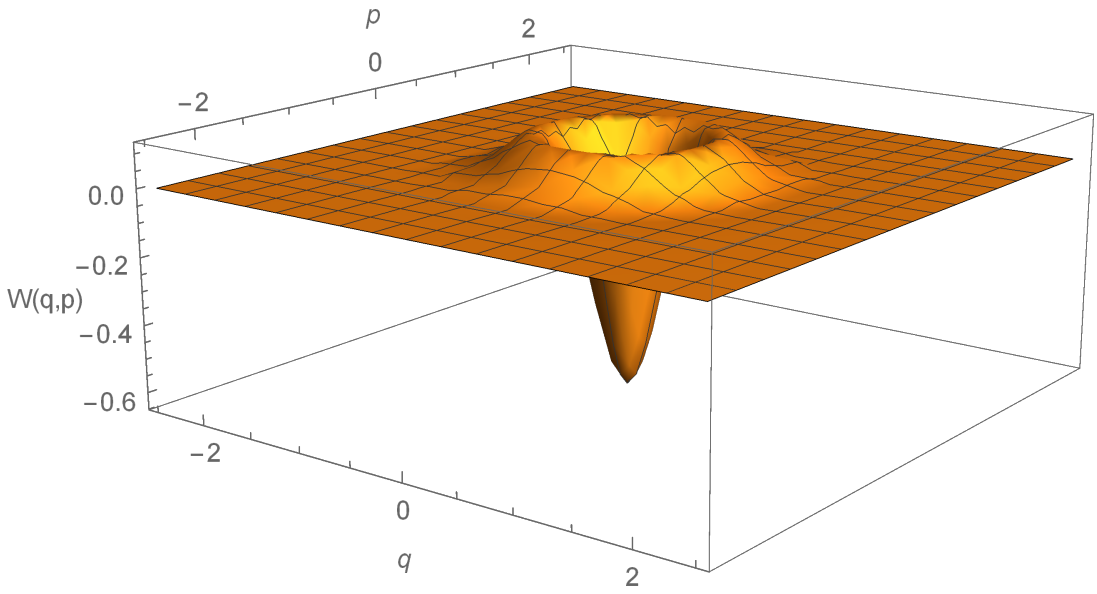

Figure 2.2: Wigner function of the Fock state $|1\rangle$. The negativity of this Wigner function demonstrates the quantumness of the state i.e. that it cannot be simulated by a classical probability distribution.

2.2.2 Coherent states

Coherent states are the eigenstates of the annihilation operator defined as

$$\hat{a}|\alpha\rangle = \alpha|\alpha\rangle,\ \alpha \in \mathbb{C}. \tag{2.22}$$

Since the Fock states form a complete basis, the coherent state can be represented as a superposition of Fock states as:

$$|\alpha\rangle = \exp\left\{\frac{-|\alpha|^2}{2}\right\} \sum_{n=0}^{\infty} \frac{\alpha^n}{\sqrt{n!}}|n\rangle. \tag{2.23}$$

The photon number distribution of a coherent state follows the Poissonian statistics. The mean number of photons in a coherent state is given as

$$\bar{n}_{|\alpha\rangle} = |\alpha|^2. \tag{2.24}$$

The expectation values of the quadrature operators for coherent states are given as:

$$\langle\alpha|\hat{X}_1|\alpha\rangle = \mathrm{Re}(\alpha), \tag{2.25}$$

$$\langle\alpha|\hat{X}_2|\alpha\rangle = \mathrm{Im}(\alpha). \tag{2.26}$$

Further, the quadrature variances are given as:

$$\langle(\Delta\hat{X}_{1,2})^2\rangle = \frac{1}{4}. \tag{2.27}$$

It is then easy to verify that coherent states minimize the uncertainty relation for quadratures given in Eq. (2.5).

Displacement operators as defined in Eq. (2.8) prove a useful tool in understanding and manipulating coherent states. Like the successive action of the annihilation operator on vacuum generates all Fock states, coherent states can be generated by the action of the displacement operator on the vacuum state as

$$\mathcal{D}(\alpha)|0\rangle = |\alpha\rangle. \tag{2.28}$$

Unlike the Fock states, the coherent states are not orthogonal, i.e,

$$\langle\beta|\alpha\rangle = \exp\left\{\frac{1}{2}(\beta^*\alpha - \beta\alpha^*)\right\}\exp\left\{-\frac{1}{2}|\beta-\alpha|^2\right\}. \tag{2.29}$$

Although not orthogonal with each other, the identity operator can be resolved in terms of coherent states as:

$$\frac{1}{\pi}\int |\alpha\rangle\langle\alpha|\, d^2\alpha = \mathbb{1}. \tag{2.30}$$

This shows that coherent states form an over-complete set. Therefore, it is possible to write any quantum state of light in the coherent state basis.

- **Characteristic functions using coherent states**

An arbitrary state of the electromagnetic field can be written in terms of coherent states using the Glauber-Sudarshan P-representation [8, 9] as

$$\hat{\rho} = \int P(\alpha)|\alpha\rangle\langle\alpha|\, d^2\alpha. \tag{2.31}$$

In particular, the P-function for a coherent state is a delta function. States of light with P-functions which are positive everywhere in phase-space or no more singular than the delta function are classical states.

A mathematical convenience of expanding states of light in the coherent basis is that it simplifies the calculation of expectation values of operators. To demonstrate this, consider the expectation value of the operator $\hat{O}$ on the state
hatrho. By the Born rule, this can be written as

$$\mathrm{Tr}[\hat{O}\hat{\rho}] = \mathrm{Tr}\left[\int \hat{O}P(\alpha)|\alpha\rangle\langle\alpha|\, d^2\alpha\right], \tag{2.32}$$

$$= \int P(\alpha)\langle\alpha|\hat{O}|\alpha\rangle\, d^2\alpha, \tag{2.33}$$

$$\equiv \pi \int P(\alpha)Q_{\hat{O}}(\alpha)\, d^2\alpha, \tag{2.34}$$

where $Q_{\hat{O}}(\alpha)$ is the Husimi Q-distribution corresponding to the operator $\hat{O}$ defined as

$$Q_{\hat{O}}(\alpha) \equiv \frac{1}{\pi}\langle\alpha|\hat{O}|\alpha\rangle. \tag{2.35}$$

The Wigner function corresponding to a coherent state $|\beta\rangle$ is gaussian, and is given as

$$W(\alpha) = \frac{2}{\pi}\exp\bigl(-2|\alpha-\beta|^2\bigr). \tag{2.36}$$

The Wigner function of a coherent state is shown in Fig. 2.3. A major advantage for using coherent states is that they are relatively easy to produce in the laboratory, as the output

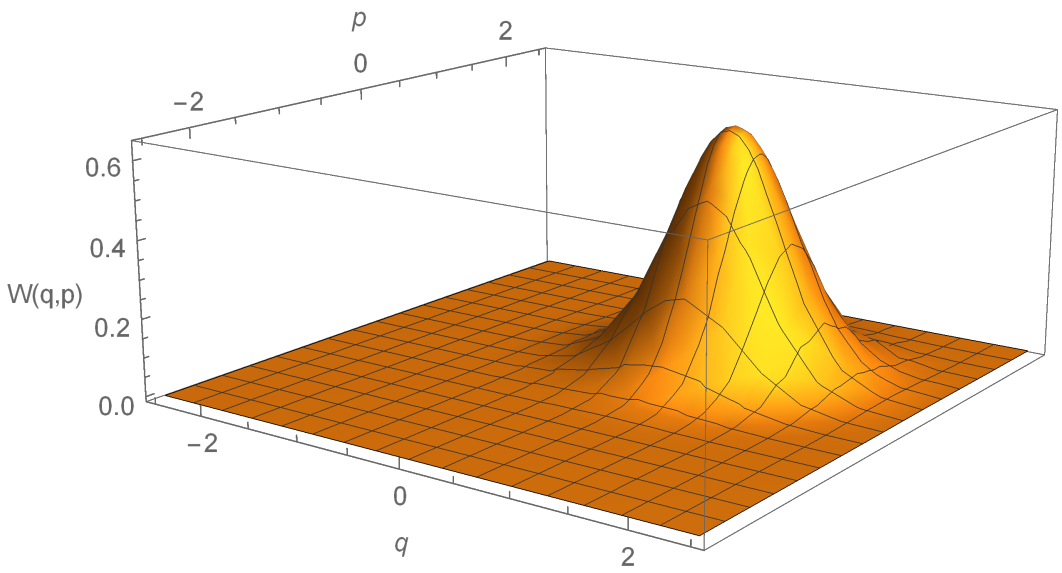

Figure 2.3: Wigner function of a coherent state $|\frac{1+i}{\sqrt{2}}\rangle$. The distribution is Gaussian centered around $\left(\frac{1}{\sqrt{2}}, \frac{1}{\sqrt{2}}\right)$.

of lasers are approximated as coherent states [10].

2.2.3 Squeezed states

Akin to the displacement operator which generates coherent states, we can define a squeezing operator which generates squeezed states as:

$$\hat{S}(\xi) = \exp\left\{\frac{1}{2}\left(\xi\hat{a}^{\dagger 2} - \xi^*\hat{a}^2\right)\right\},\ \xi = re^{i\phi}, \tag{2.37}$$

where ξ is called the squeezing parameter. The action of the squeezing operator on the vacuum generates the squeezed vacuum state. Expanded in terms of Fock states, the squeezed vacuum state is:

$$|\xi\rangle = \frac{1}{\sqrt{\cosh r}} \sum_{n=0}^{\infty} e^{in\phi} (\tanh r)^n \frac{\sqrt{(2n)!}}{(n!)^2 2^{2n}} |2n\rangle. \tag{2.38}$$

The squeezed vacuum state is a superposition of only even number of photons. The mean number of photons in this state is given as

$$\bar{n}_{|\xi\rangle} = \sinh^2(r). \tag{2.39}$$

For squeezed vacuum states, the expectation values of the quadratures vanish, and the quadrature uncertainties are given as

$$\langle(\Delta\hat{X}_1)^2\rangle = \frac{1}{4}e^{2r}, \tag{2.40}$$

$$\langle(\Delta\hat{X}_2)^2\rangle = \frac{1}{4}e^{-2r}. \tag{2.41}$$

Thus we see that squeezed vacuum states are also minimum uncertainty states as given in Eq. (2.5)).

The Wigner function corresponding to squeezed vacuum is gaussian and is given as

$$W(\alpha) = \frac{2}{\pi}\exp\left[-\frac{1}{2}\left(e^{-2r}\,\mathrm{Re}(\alpha)^2 + e^{2r}\,\mathrm{Im}(\alpha)^2\right)\right], \tag{2.42}$$

where the squeezing angle $\theta = 0$. The Wigner function of a squeezed vacuum state is shown in Fig. 2.4.

2.2.4 Thermal states

Thermal states of the electromagnetic field are those that are at equilibrium at a given temperature. They are mixed states, which are described not by a state vector, but by a density matrix.

Consider a single-mode thermal radiation of frequency ω in thermal equilibrium with a cavity at a temperature T. The density matrix corresponding to a thermal state of a

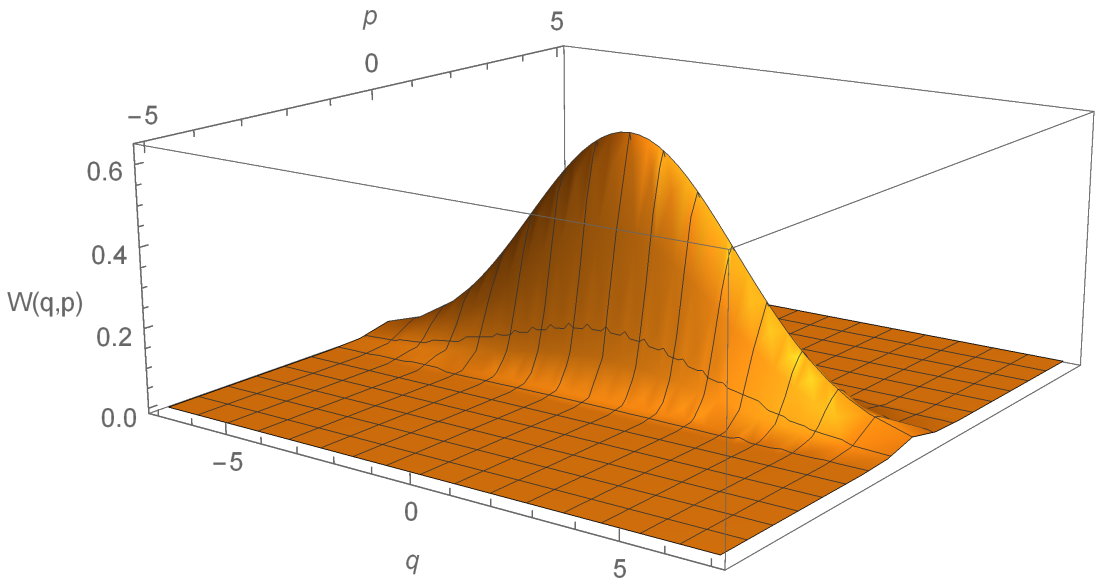

Figure 2.4: Wigner function of a squeezed vacuum state with squeezing parameter $\xi = 1$. Notice that the Wigner function looks squeezed.

Hamiltonian $\hat{H}$ at a temperature T is given as:

$$\hat{\rho}_{\mathrm{Th}} = \frac{\exp\left(-\frac{\hat{H}}{k_b T}\right)}{\mathrm{Tr}\left[\exp\left(-\frac{\hat{H}}{k_b T}\right)\right]}, \tag{2.43}$$

where k_B is the Boltzmann constant. For a single mode electromagnetic field, substituting the expression for the Hamiltonian as given in Eq. (1.15) in Eq. (2.43), we obtain the Fock-state expansion of the thermal state as:

$$\hat{\rho}_{\mathrm{Th}} = \frac{1}{1+\bar{n}} \sum_{n=0}^{\infty} \left(\frac{\bar{n}}{1+\bar{n}}\right)^n |n\rangle\langle n|, \tag{2.44}$$

where the mean number of photons in the thermal state is given as

$$\bar{n} = \frac{1}{\exp\left(\frac{\hbar\omega}{k_B T}\right) - 1}. \tag{2.45}$$

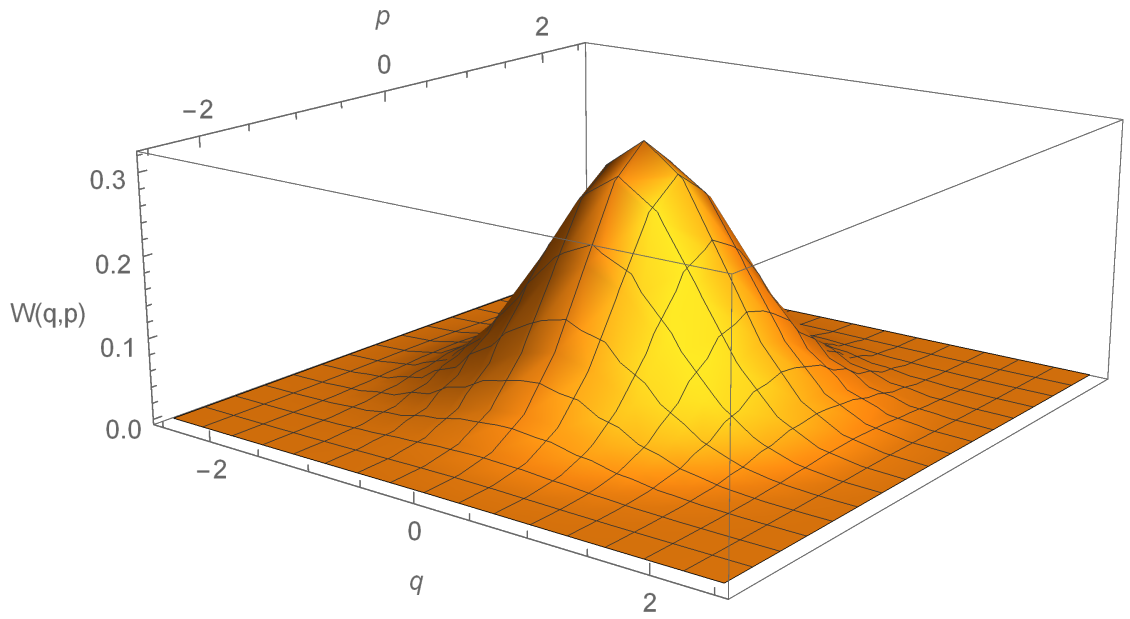

Figure 2.5: Wigner function of a thermal state with mean photon number $\bar{n} = 1$. The Wigner function is Gaussian and is centered at the origin.

Thermal states are also gaussian with Wigner functions given as

$$W(\alpha) = \frac{2}{\pi(\bar{n}+1)} \exp\left(-\frac{2|\alpha|^2}{\bar{n}+1}\right). \tag{2.46}$$

The Wigner function of a thermal state is shown in Fig. 2.5.

2.3 Evolution of quantum optical states

In the previous section we talked about quantum states of light. In this section we will see how quantum states of light evolve via optical elements. In this section, I will use the terms optical elements, optical systems, and optical devices interchangeably.

Consider a multimode optical element with mode creation and annihilation operators $\hat{a}_j^\dagger$ and $\hat{a}_j$ respectively, where $j = 1, \ldots, N$. These operators satisfy the commutation relations

$$[\hat{a}_j, \hat{a}_k^\dagger] = \delta_{j,k}, \tag{2.47}$$

$$[\hat{a}_j, \hat{a}_j] = 0, \tag{2.48}$$

$$[\hat{a}_j^\dagger, \hat{a}_j^\dagger] = 0. \tag{2.49}$$

The Hamiltonian corresponding to this optical element can then be written as a function of the the mode operators. This Hamiltonian generates the evolution of the optical state through the optical element.

In general, the evolution of a state of light is described by Eq. (1.1) or Eq. (1.2) depending on whether the light is in a pure or a mixed state. However, a direct application of these formulae may prove cumbersome in many cases as the Hilbert space corresponding to even a single mode of light is infinite dimensional, and as the Hamiltonian might have a complicated structure. Simplifications are possible when we restrict our attention to particular classes of states and Hamiltonians.

In this section, we will restrict our attention to Hamiltonians which are at most quadratic in the mode creation and annihilation operators. The resulting class of evolutions are called gaussian evolutions. Under gaussian evolutions, simplifications arise from the fact that in such optical elements, in the Heisenberg picture, the evolution of mode operators due to these elements are linear.

We will first discuss linear optics, which arises when the interaction Hamiltonian corresponding to an optical element is bilinear in the mode operators. We will then discuss optical elements whose interaction terms are quadratic in the mode operators. This section follows Ref. [5] and Ref. [11].

2.3.1 Linear optics

When the interaction Hamiltonian of an optical element is bilinear in the mode creation and annihilation operators, then such elements are referred to as linear-optical elements. In

general, the Hamiltonian corresponding to a N-mode linear optical element is Hermitian, and can be written as

$$\hat{H} = \sum_{j,k=1}^{N} A_{jk} \hat{a}_j^\dagger \hat{a}_k. \tag{2.50}$$

It can be easily verified that a Hamiltonian of this form commutes with the total photon number operator. This implies that the total number of photons is conserved during the evolution with such an operator.

For a linear optical element, in the Heisenberg picture, the mode operators evolve as

$$\hat{a}_i^{'\dagger} \to U_{ij} \hat{a}_j^\dagger, \tag{2.51}$$

where the repeated indices are summed over, and where U is unitary.

I will now introduce the building blocks of linear optical elements, namely phase shifters and beam splitters. These optical elements can be used to generate any arbitrary linear optical system. In Ref. [12], an arbitrary linear optical system was exactly decomposed into a sequence of beam splitters and phase shifters, using $O(n^2)$ of these elements. In contrast, Ref. [13] uses an alternate decomposition with Mach-Zehnder interferometers as its building blocks. This decomposition is more resilient to optical losses.

- **Phase shifter**

The simplest linear optical element is a single mode element named the phase shifter. The (dimensionless) Hamiltonian of a phase shifter is

$$\hat{H}_\phi = \phi\, \hat{a}^\dagger \hat{a}, \tag{2.52}$$

where ϕ is the phase shift produced by the element, and $\hat{a}^\dagger$ abd $\hat{a}$ are the mode operators. In Heisenberg picture, the mode operators of a phase shifter evolve as

$$\hat{a}_{\text{out}}^\dagger = e^{-i\phi} \hat{a}_{\text{in}}^\dagger. \tag{2.53}$$

Substituting Eq. (2.53) in Eq. (2.14), we see that under the action of a phase shifter, a Fock state evolves as

$$|n\rangle \to e^{in\phi}|n\rangle. \tag{2.54}$$

Using Eq. (2.54) in Eq. (2.23) we see that a coherent state evolve via phase shifters by acquiring the phase of the phase shifter as

$$|\alpha\rangle \to |e^{i\phi}\alpha\rangle. \tag{2.55}$$

In practice, a phase shifter achieves its transformation by modifying the optical path length. This is typically done by introducing a transparent material with a different refractive index than that of other modes of light.

- **Beam splitter**

A beam splitter is a two-mode optical element which interferes light in its input modes. The (dimensionless) Hamiltonian a beam splitter is

$$\hat{H} = \theta\,(e^{i\phi}\hat{a}_1^\dagger\hat{a}_2 + e^{-i\phi}\hat{a}_1\hat{a}_2^\dagger), \tag{2.56}$$

where $\hat{a}_{1,2}$ are the mode operators, and θ determines the reflection and transmission coefficients of the beamsplitter. This Hamiltonian also commutes with the total number operator, so that the total number of photons is preserved during the evolution via a beam splitter.

In this thesis, I will use 50:50 beam splitters. The prefix '50:50' arises from the fact that the reflection and transmission coefficients of this beam splitter are both 50%. Such a beamsplitter can be parametrized with $\theta = \frac{\pi}{4}$ and $\phi = \frac{\pi}{2}$. Note that other choices of ϕ — in particular $\phi = 0$ — is equally valid and is used in the literature.

In the Heisenberg picture, the mode operators of a 50:50 beam splitter evolve as

$$\begin{pmatrix} \hat{a}_1^\dagger \\ \hat{a}_2^\dagger \end{pmatrix}_{\text{out}} = \frac{1}{\sqrt{2}} \begin{pmatrix} 1 & -i \\ -i & 1 \end{pmatrix} \begin{pmatrix} \hat{a}_1^\dagger \\ \hat{a}_2^\dagger \end{pmatrix}_{\text{in}}. \tag{2.57}$$

Under the action of a beam splitter, a coherent state evolves as

$$|\alpha\rangle_1 \to \left|\frac{\alpha}{\sqrt{2}}\right\rangle_1 \left|\frac{i\alpha}{\sqrt{2}}\right\rangle_2. \tag{2.58}$$

In practice, a beam splitter is a partially reflective mirror.

2.3.2 Quadratically non-linear optics

In contast to that of linear optical elements, the Hamiltonian of a quadratically non-linear optical element has terms quadratic in the mode operators. For such elements, the mode operators evolve as

$$\hat{a}_i^\dagger = U_{ij}\hat{b}_j^\dagger + V_{ij}\hat{b}_j, \tag{2.59}$$

where $\hat{a}$ represents the input mode operators, $\hat{b}$ represents the output mode operators, and $UU^\dagger - VV^\dagger = \mathbb{1}$. Such transformations are called Bogoliubov transformations, and give rise to purely quantum phenomena such as squeezing. In particular, under the action of the squeezing operator given in Eq. (2.37), the mode operators evolve as

$$\hat{b}^\dagger = \cosh(r)\,\hat{a}^\dagger - e^{-i\phi}\sinh(r)\,\hat{a}, \tag{2.60}$$

where $\hat{a}$ and $\hat{b}$ are the input and output mode operators respectively.

2.4 Quantum detectors

The final step in any experiment involving quantum states is the detection process. In this step, a suitable measurement is performed on a quantum state so as to obtain a result. The distinguishing feature of quantum measurements are that they are inherently probabilistic.

Mathematically, any detector is completely described by a set of measurement operators $\{\hat{M}_k\}$ called Positive Operator Valued Measures (POVMs). When such a device measures a quantum state $\hat{\rho}$, the probability of observing a particular outcome k is given by the Born rule as

$$p(k)_\rho = \mathrm{Tr}[\hat{\rho}\hat{M}_k]. \tag{2.61}$$

Since probabilities are non-negative, POVM elements are positive semi-definite. Further, since probabilities of all possible detection outcomes sum to one, POVM elements satisfy the completeness criterion that

$$\sum_{k=0}^{K-1} \hat{M}_k = \mathbb{1}, \tag{2.62}$$

where the index k labels the POVM element of which there are K present. This implies that a set of POVM elements completely describes the measurement device.

A particularly interesting detector is the photon-number-resolving detector. For such a detector, the POVM elements are projectors onto definite photon number states i.e. $\{|n\rangle\langle n|,\ n = 0, 1, 2 \ldots\}$. Two other common detectors are the homodyne detector and the heterodyne detector. These detectors perform Gaussian measurements, meaning that when Gaussian states of light are input, their outcomes are Gaussian-distributed. In the case of homodyne detection, the POVM set consists of projectors onto all position or momentum eigenstates. In contrast, the POVM set in the case of heterodyne detection consists of projectors onto all coherent states.

As in the case of quantum states of light, one can also use Wigner functions to visualize POVM elements.

2.5 Gaussian quantum information

A state of light completely described by the first and the second moments of the quadrature operator given in Eq. (2.2) is called a Gaussian state of light. The name 'Gaussian' arises from the fact that the Wigner function corresponding to such a state

of light is Gaussian. When a Gaussian state of light evolves via a Hamiltonian that is at most quadratic in the mode operators, these states remain Gaussian. Therefore such evolutions are called Gaussian evolutions. In this section, I will introduce a formalism for manipulating gaussian states of light as well as gaussian evolutions of them.

2.5.1 Gaussian states

Consider a system of light of n bosonic modes. Akin to Eq. (2.2), I define the quadrature operators corresponding to the mode k as

$$\hat{q}_k \equiv \hat{a}_k + \hat{a}_k^\dagger, \tag{2.63}$$

$$\hat{p}_k \equiv i(\hat{a}_k - \hat{a}_k^\dagger), \tag{2.64}$$

where $\hat{a}_k$ and $\hat{a}_k^\dagger$ are the mode annihilation and creation operators respectively. Note that the above definition differs from the definition in Eq. (2.2) by only an overall factor. I then define the vector of quadrature operators of length $2n$ as

$$\hat{\mathbf{x}} \equiv (\hat{q}_1, \ldots, \hat{q}_n, \hat{p}_1, \ldots, \hat{p}_n)^T. \tag{2.65}$$

As mentioned earlier, the first and the second moments of the quadrature operators fully characterize a Gaussian state. For a state of light described by the density matrix ρ, the first moments are given by the mean vector as

$$\bar{\mathbf{x}} \equiv \langle \hat{\mathbf{x}} \rangle \equiv \mathrm{Tr}[\hat{\mathbf{x}}\hat{\rho}]. \tag{2.66}$$

The second moments are given by the covariance matrix defined as

$$V_{ij} \equiv \frac{1}{2}\langle \hat{x}_i \hat{x}_j + \hat{x}_j \hat{x}_i \rangle - \langle \hat{x}_i \rangle \langle \hat{x}_j \rangle. \tag{2.67}$$

Notable examples of Gaussian states include coherent states, thermal states, squeezed

states, as well as the vacuum state. A remarkable exclusion from the list of Gaussian states are the Fock states. We will now see how some common Gaussian states are characterized.

- **Coherent states**

As an example, let us calculate the mean vector and the covariance matrix of a coherent state. For a coherent state $|\alpha\rangle$, the mean vector is given as

$$\bar{\mathbf{x}}_{|\alpha\rangle} = \begin{pmatrix} \langle \hat{a} + \hat{a}^\dagger \rangle \\ i\langle \hat{a} - \hat{a}^\dagger \rangle \end{pmatrix} = \begin{pmatrix} 2\mathrm{Re}(\alpha) \\ 2\mathrm{Im}(\alpha) \end{pmatrix} \tag{2.68}$$

Further, the covariance matrix representing a coherent state is

$$V_{|\alpha\rangle} = \begin{pmatrix} 1 & 0 \\ 0 & 1 \end{pmatrix}. \tag{2.69}$$

- **Squeezed vacuum state**

For a squeezed vacuum state, the mean vector is given as

$$\bar{\mathbf{x}}_{|\xi\rangle} = \begin{pmatrix} 0 \\ 0 \end{pmatrix}. \tag{2.70}$$

Further, its covariance matrix is

$$V_{|\xi\rangle} = \begin{pmatrix} \cosh 2r - \sinh 2r \cos\theta & -\sinh 2r \sin\theta \\ -\sinh 2r \sin\theta & \cosh 2r + \sinh 2r \cos\theta \end{pmatrix}, \tag{2.71}$$

where the squeezing parameter $\xi = re^{i\theta}$. When $\theta = 0$, the covariance matrix reduces to

$$V_{|\xi=|r|\rangle} = \begin{pmatrix} \exp(-2r) & 0 \\ 0 & \exp(2r) \end{pmatrix}. \tag{2.72}$$

2.5.2 Gaussian evolutions

Having discussed how Gaussian states are characterized, we now discuss a formalism for describing the evolution of such states. If the Hamiltonian that evolves Gaussian states remain at most quadratic in the quadrature operators, then the state remains Gaussian. Therefore, such evolutions are called Gaussian evolutions, and can be characterized by how it evolves the covariance matrix and the mean vector of light.

Under a Gaussian evolution, the mean vector and the covariance matrix of a state of light evolves as

$$\bar{\mathbf{x}} \to S\bar{\mathbf{x}} + d, \tag{2.73}$$

$$V \to SVS^T, \tag{2.74}$$

where the parameters (S, d) characterize the Gaussian evolution. Therefore, specifying these parameters completely specifies the evolution.

For a linear optical system the evolution of the mode operators obtains a simpler form. This can be seen as follows: Consider a linear optical system which transforms the mode operators as

$$(a_i^\dagger)_{\text{out}} = U_{ij}\,(a_j^\dagger)_{\text{in}}, \tag{2.75}$$

where the Einstein summation convention is followed. The above relation can be rewritten to obtain the evolution of the position quadrature as

$$\begin{aligned}
(\hat{q}_i)_{\text{out}} &= U_{ij}\,(\hat{a}_j^\dagger)_{\text{in}} + {U_{ij}}^*\,(\hat{a}_j)_{\text{in}} && (2.76)\\
&= [\text{Re}(U_{ij}) + i\text{Im}(U_{ij})]\,(\hat{a}_j^\dagger)_{\text{in}} + [\text{Re}(U_{ij}) - i\text{Im}(U_{ij})]\,(\hat{a}_j)_{\text{in}} && (2.77)\\
&= \text{Re}(U_{ij})(\hat{a}_j^\dagger + \hat{a}_j)_{\text{in}} + i\text{Im}(U_{ij})(\hat{a}_j^\dagger - \hat{a}_j)_{\text{in}} && (2.78)\\
&= \text{Re}(U_{ij})(\hat{q}_i)_{\text{in}} + \text{Im}(U_{ij})(\hat{p}_i)_{\text{in}}. && (2.79)
\end{aligned}$$

Similarly, the evolution of the momentum quadrature can be obtained as

$$(\hat{p}_i)_{\text{out}} = -\text{Im}(U_{ij})(\hat{q}_i)_{\text{in}} + \text{Re}(U_{ij})(\hat{p}_i)_{\text{in}}. \tag{2.80}$$

Combining Eqs. (2.79) and (2.80) and evaluating the expectation values of the operators, we obtain the evolution of the mean vector as

$$\bar{\mathbf{x}}_{\text{out}} = S_U \, \bar{\mathbf{x}}_{\text{in}} \tag{2.81}$$

where

$$S_U = \begin{pmatrix} \text{Re}(U) & \text{Im}(U) \\ -\text{Im}(U) & \text{Re}(U) \end{pmatrix} \tag{2.82}$$

Comparing Eqs. (2.73) and (2.81), we observe that for passive linear optical elements such as beamsplitters or phase shifters, $d = 0$.

We will now discuss how phase shifters and beamsplitters are characterized in this formalism. From Eq. (2.53), the action of a phase shifter with a phase angle ϕ can be characterized with

$$S_\phi = \begin{pmatrix} \cos\phi & -\sin\phi \\ \sin\phi & \cos\phi \end{pmatrix}. \tag{2.83}$$

Similarly, noting Eq. (2.57), a 50:50 beamsplitter can be characterized with

$$S_{BS} = \frac{1}{\sqrt{2}} \begin{pmatrix} 1 & 0 & 0 & -1 \\ 0 & 1 & -1 & 0 \\ 0 & 1 & 1 & 0 \\ 1 & 0 & 0 & 1 \end{pmatrix} \tag{2.84}$$

- **Wick's theorem**

Higher moments of a Gaussian state can be obtained from the first and second moments of the Gaussian state via the Wick's theorem [14, 15]. For arbitrary operators $\hat{O}_i$ of a

Gaussian quantum state, the third and fourth moments are evaluated as

$$\langle \hat{O}_1\hat{O}_2\hat{O}_3\rangle = \underbrace{\hat{O}_1\hat{O}_2}\,\langle \hat{O}_3\rangle + \underbrace{\hat{O}_1\hat{O}_3}\,\langle \hat{O}_2\rangle + \underbrace{\hat{O}_2\hat{O}_3}\,\langle \hat{O}_1\rangle + \langle \hat{O}_1\rangle\langle \hat{O}_2\rangle\langle \hat{O}_3\rangle, \tag{2.85}$$

$$\langle \hat{O}_1\hat{O}_2\hat{O}_3\hat{O}_4\rangle = \underbrace{\hat{O}_1\hat{O}_2}\,\underbrace{\hat{O}_3\hat{O}_4} + \underbrace{\hat{O}_1\hat{O}_3}\,\underbrace{\hat{O}_2\hat{O}_4} + \underbrace{\hat{O}_1\hat{O}_4}\,\underbrace{\hat{O}_2\hat{O}_3} + \langle \hat{O}_1\rangle\langle \hat{O}_2\rangle\langle \hat{O}_3\rangle\langle \hat{O}_4\rangle, \tag{2.86}$$

where $\underbrace{\hat{O}_i\hat{O}_j}$ is the contraction of operators defined as

$$\underbrace{\hat{O}_i\hat{O}_j} \equiv \langle \hat{O}_i\hat{O}_j\rangle - \langle \hat{O}_i\rangle\langle \hat{O}_j\rangle. \tag{2.87}$$

Even higher moments of the Gaussian state can be found by the repetitive application of Eqs. (2.85) and (2.86).

2.6 Quantum metrology

Having discussed how various quantum states, processes, and detectors are characterized, I will now briefly introduce the task of phase estimation. I will first introduce the Mach-Zehnder interferometer and then show how it can be used to achieve this task. I will then introduce various schemes for phase estimation and introduce metrics such as the shot-noise limit and the Heisenberg limit. The task of phase estimation involves figuring out an unknown phase, while keeping the uncertainty in the phase estimated to a minimum. This is typically done via interferometry.

The archetype of interferometers is the Mach-Zehnder interferometer shown in Fig. 2.6. It consists of two ports into which different states of light can be input. The input light is then mixed at a 50:50 beamsplitter. In one of the two paths that light can take after the beamsplitter is the phase — the parameter to be measured. This phase imparts a phase shift to light incident on it so that information about this phase shift is encoded in the light. This information is retrieved by performing a suitable measurement on the states of light after it passes through another 50:50 beamsplitter. The past several decades have seen various strategies being employed in order to precisely measure the phase shift imparted to light [16].

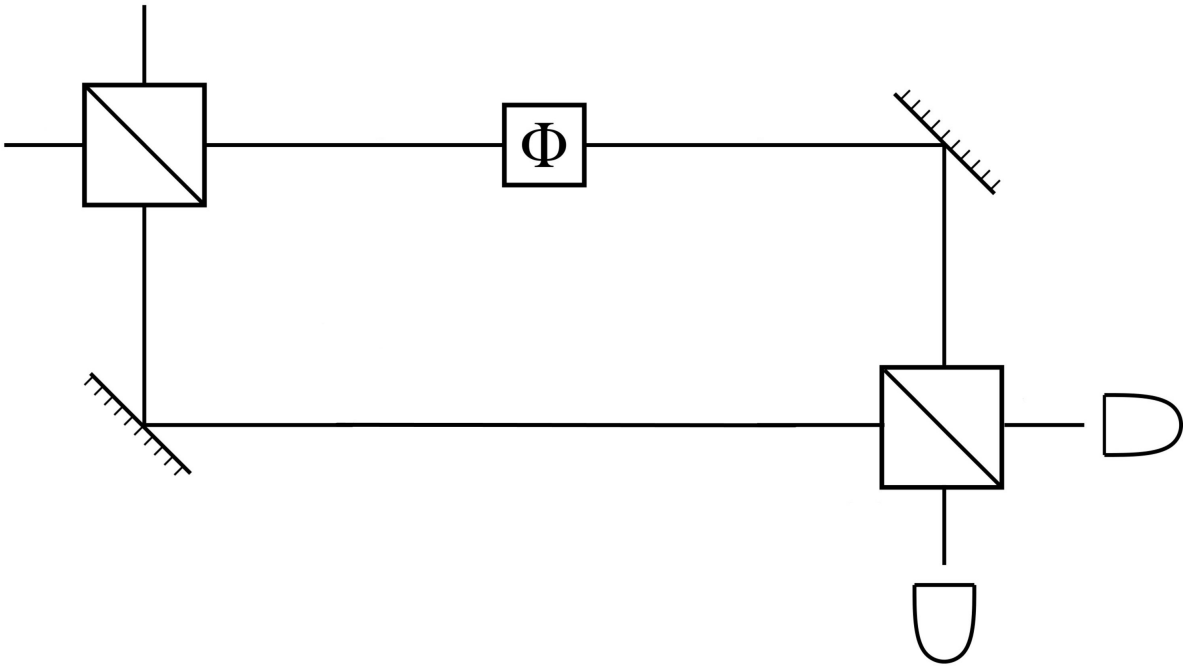

Figure 2.6: A schematic of a Mach-Zehnder interferometer for measuring the phase shift ϕ.

For a measurement operator $\hat{O}$, the uncertainty in phase can simply be calculated via the error propagation formula as

$$\Delta\phi = \frac{\Delta\hat{O}}{\left|\frac{\partial\langle\hat{O}\rangle}{\partial\phi}\right|}, \tag{2.88}$$

where $\langle\Delta\hat{O}\rangle$ represents the standard deviation of the operator $\hat{O}$ given as $\sqrt{\langle\hat{O}^2\rangle - \langle\hat{O}\rangle^2}$ [5].

Let us briefly discuss a few examples of doing phase estimation with various states of light.

- **Coherent and Vacuum**

Consider a scenario of phase estimation with inputs being a coherent state $|\alpha\rangle$ and the vacuum state $|0\rangle$. In this case, the precision in phase estimation is given as

$$\Delta\phi = \frac{1}{|\alpha|} = \frac{1}{\sqrt{\bar{n}}}, \tag{2.89}$$

where $\bar{n}$ is the total number of photons input. This limit is called the shot noise limit. Improvements to this limit are possible if we use other states of light as probes.

- **Coherent and Squeezed vacuum**

If we use coherent state and squeezed vacuum as inputs to the Mach-Zehnder interferometer, then we can measure the unknown phase more precisely. For this, we choose the squeezing parameter such that $\sqrt{n}/2$ of the average n photons are in the squeezed state. When the mean photon number is large, the phase difference can be calculated from measuring the intensity difference between the two output ports. In this case, the precision in phase estimation is given as

$$\Delta\phi = \frac{1}{|\alpha|} = \frac{1}{\bar{N}^{3/4}}. \tag{2.90}$$

Thus, by using squeezed vacuum over vacuum in one port, we are able to beat the shot noise limit.

- **N00N states**

The precision in phase estimation can be further improved if we use states of definite photon number which are maximally path-entangled such as

$$\Psi\rangle = \frac{|N\rangle|0\rangle + |0\rangle|N\rangle}{\sqrt{2}}. \tag{2.91}$$

In this case, the precision of phase estimation reaches the Heisenberg limit as

$$\Delta\phi = \frac{1}{N}. \tag{2.92}$$

2.7 Summary

In this chapter, I have introduced the mathematical description of the elements of quantum optics — states of light, processes that manipulate light, and detectors which detect light. I also briefly introduced the formalism of Gaussian quantum information.

Finally, I introduced quantum metrology showing examples of how quantum light improves the precision of parameter estimation.

Chapter 3
Direct Characterization of Linear and Quadratically Nonlinear Optical Systems

In this chapter, I will develop a method to characterize optical systems. After motivating the problem, I will introduce the proposed setup for characterizing optical systems. I will then show how this setup can be used to characterize linear evolutions. I will then discuss the sensitivity of this scheme. I will also demonstrate that advantages in sensitivity gains from quantum parameter estimation do not carry over to this scenario. I will then move on to discuss how this setup can be used to characterize quadratically nonlinear optical systems. Finally, I will model optical losses in such systems as well as develop a method to characterize such losses. [1]

3.1 Introduction

Characterizing quantum evolutions is one of the central tasks in quantum-information processing. Quantum process tomography is an indispensable tool in the characterization of such evolutions. In general, the evolution of a N-dimensional quantum system is a completely positive trace-preserving map, which is characterized by $O(N^4)$ real parameters [17]. In addition to standard quantum process tomography [18, 19], various schemes such as ancilla-assisted process tomography [20, 21], direct characterization of quantum dynamics [22, 23] and compressed sensing [24] have been developed to characterize such maps. A resource analysis of some of these schemes are found in Ref. [25].

Characterizing evolutions in optical systems require a different scheme as the Hilbert space corresponding to such systems is infinite dimensional. Several schemes have been proposed for characterizing optical systems. In Ref. [26], optical systems were probed with coherent states, and the results were used to predict the action of the system on an ar-

[1] Parts of this chapter previously appeared as Kevin Valson Jacob, Anthony E. Mirasola, Sushovit Adhikari, and Jonathan P. Dowling, Phys. Rev. A **98**, 052327 (2018). It is reprinted by permission of American Physical Society.

bitrary state of light using the Glauber-Sudarshan P-representation [8, 9]. However, the P-function is highly singular for non-classical inputs, which can yield inaccuracies in the process reconstruction. To alleviate this problem, maximum likelihood estimation was used in Refs. [27, 28] to recreate the process tensor in the Fock basis. Another approach, based on measurement of normally-ordered moments using coherent probes, was performed in Ref. [29].

Simpler schemes are possible when we restrict our attention to linear optics. Such systems have been found to have a variety of applications ranging from interferometry, quantum metrology [30], linear optical quantum computing [31], and boson sampling [32]. In such systems, the mode operators evolve unitarily, and characterizing the corresponding finite dimensional unitary matrix completely specifies the evolution.

Several schemes for characterizing linear-optical devices were developed in Refs. [33, 34, 35]. In Ref. [33], single-photon probes were used to find the moduli of all matrix elements, and two-photon coincidence probabilities were used to find all the phases of the matrix elements of a d-mode unitary transformation. A similar scheme was analyzed in detail in Ref. [34], which increased the accuracy in characterization by accounting for mode mismatch errors. Another approach using coherent state probes instead of single photons was developed in Ref. [35]. An approach based on numerical global optimization of parameters was undertaken in Ref. [36]. Finally, in Ref. [37], a genetic algorithm was used to characterize unitary transformations.

However, some of these schemes assumed that the unitary matrix is real-bordered i.e. that the elements in the first row and first column of the matrix were real. This restricts the class of devices that we can characterize. For instance, we would not be able to characterize a single-mode phase shifter by these schemes. In general, the phases in the first row and column would be relevant when either the input state is superposed across input modes or when there is further interferometry after the device.

The restriction on the class of unitaries which could be characterized in these schemes

stems from the fact that in quantum mechanics, only phase differences and not phases themselves can be measured. Thus in order to find all the phases in the transformation matrix, at least one auxillary mode must be introduced relative to which all phases can be measured. We will show that a modified Mach-Zehnder interferometer serves this purpose.

Although characterizing linear optical devices has been explored, not much attention has been given to characterizing nonlinear devices. Such devices have been shown to be useful in producing squeezed light [38] and entangled photons [39]. Systems where the Hamiltonian is quadratic in the mode operators produce the well-known Boguliubov transformations of the mode operators [40]. Such processes map Gaussian states to Gaussian states [41, 42], and are therefore referred to as Gaussian processes. In Ref. [43], the problem of Gaussian process tomography was reduced to Gaussian state tomography, for which there exist efficient methods [44]. Using this scheme, a N-mode Gaussian process can be characterized by a tomographic procedure using $O(N^2)$ coherent-state probes.

In this paper, we present an alternate scheme to characterize Gaussian processes. In our scheme, the task of state tomography is eliminated, as we will directly be able to obtain the transformation matrix of the mode operators. However, there is a trade-off with the resource requirements of our scheme. In the case of characterizing linear optics, there is no additional resource requirement as $O(N^2)$ coherent state probes suffice. However, in order to characterize quadratically non-linear processes also, we additionally require $O(N^2)$ single photons. A wide range of single photon sources and detectors are experimentally available [45]. We will see that the proposed setup is similar to that in Ref. [35] but with an auxillary mode introduced.

3.2 Setup

A schematic of the proposed modified Mach-Zehnder interferometer is shown in Fig. 3.1. It consists of two 50:50 beam splitters, a phase shifter, the unknown device to be characterized, and photodetectors. One of the input and output modes of the unknown device is placed in the lower arm of the interferometer; and the phase shifter is placed

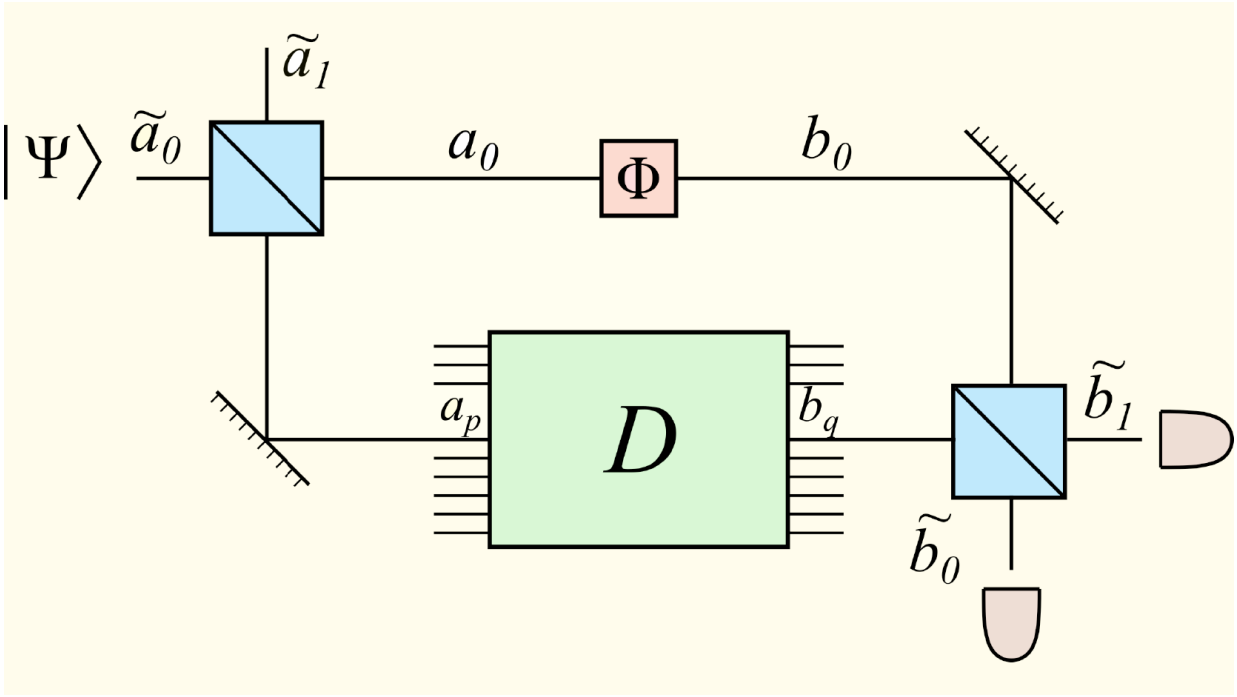

Figure 3.1: Modified Mach-Zehnder interferometer for characterizing an unknown device D. The p^{th} input and q^{th} output modes of the device D is inserted in the lower arm of the interferometer. The upper arm consists of a phase shifter which introduces a phase of 0 or $\frac{\pi}{2}$ to its input. The modes are labeled as shown.

in the upper arm of the interferometer. The input modes of the first beam splitter and the output modes of the second beamsplitter are labelled as $\tilde{a}_i$ and $\tilde{b}_i$, respectively where $i = 0, 1$. The first beamsplitter implements the transformation,

$$\begin{pmatrix} \hat{\tilde{a}}_0^\dagger \\ \hat{\tilde{a}}_1^\dagger \end{pmatrix} = \frac{1}{\sqrt{2}} \begin{pmatrix} 1 & i \\ i & 1 \end{pmatrix} \begin{pmatrix} \hat{a}_0^\dagger \\ \hat{a}_p^\dagger \end{pmatrix}. \tag{3.1}$$

Here a_p is the p^{th} input mode of the unknown device, which is coupled to the lower arm of the interferometer. The upper mode consists of a phase shifter which implements the transformation

$$\hat{a}_0^\dagger = e^{i\phi} \hat{b}_0^\dagger, \tag{3.2}$$

where $\phi \in \{0, \frac{\pi}{2}\}$. The output mode b_q of the device and mode b_0 transform in the second beam splitter as

$$\begin{pmatrix} \hat{b}_0^\dagger \\ \hat{b}_q^\dagger \end{pmatrix} = \frac{1}{\sqrt{2}} \begin{pmatrix} 1 & i \\ i & 1 \end{pmatrix} \begin{pmatrix} \hat{\tilde{b}}_0^\dagger \\ \hat{\tilde{b}}_1^\dagger \end{pmatrix}. \tag{3.3}$$

3.3 Characterization of unitary transformations

Consider a N-mode passive linear optical device where the input and output modes are labeled as a_i and b_i respectively where $i \in \{1, 2, ...N\}$. The input mode and output mode creation operators are related by a unitary transformation as

$$\hat{a}_i^\dagger = U_{ij} \hat{b}_j^\dagger, \tag{3.4}$$

where it is implicit that the repeated index is summed over. Our aim is to fully characterize this unitary matrix.

For this, we probe it with coherent states. Consider a coherent state input in mode $\tilde{a}_0$. The input state is

$$|\Psi\rangle = \hat{\mathcal{D}}_{\tilde{a}_0}(\alpha)|0\rangle = e^{\alpha \hat{\tilde{a}}_0^\dagger - \alpha^* \hat{\tilde{a}}_0}|0\rangle, \tag{3.5}$$

where α is arbitrarily chosen, and $\hat{\mathcal{D}}_{\tilde{a}_0}$ is the displacement operator acting on mode $\tilde{a}_0$. After the first beam splitter, this state is

$$|\Psi\rangle = \hat{\mathcal{D}}_{a_0}\left(\frac{\alpha}{\sqrt{2}}\right) \otimes \hat{\mathcal{D}}_{a_p}\left(\frac{i\alpha}{\sqrt{2}}\right)|0\rangle. \tag{3.6}$$

After the unitary device and the phase shifter, this state is transformed as

$$|\Psi\rangle = \hat{\mathcal{D}}_{b_0}\left(\frac{e^{i\phi}\alpha}{\sqrt{2}}\right) \otimes_{j=1}^{N} \exp\left[\frac{i\alpha U_{pj}\hat{b}_j^\dagger}{\sqrt{2}} + \frac{i\alpha U_{pj}^* \hat{b}_j}{\sqrt{2}}\right]|0\rangle. \tag{3.7}$$

This can be rewritten as

$$|\Psi\rangle = \hat{\mathcal{D}}_{b_0}\left(e^{i\phi}\frac{\alpha}{\sqrt{2}}\right) \otimes \hat{\mathcal{D}}_{b_q}\left(\frac{i\alpha U_{pq}}{\sqrt{2}}\right) \otimes_{j\neq q} \hat{\mathcal{D}}_{b_j}\left(\frac{i\alpha U_{pj}}{\sqrt{2}}\right)|0\rangle. \tag{3.8}$$

After the final beam splitter, the reduced state in modes $\tilde{b}_0$ and $\tilde{b}_1$ is

$$|\tilde{\Psi}\rangle = \hat{\mathcal{D}}_{\tilde{b}_0}\left(\frac{\alpha}{2}(e^{i\phi} - U_{pq})\right) \otimes \hat{\mathcal{D}}_{\tilde{b}_1}\left(\frac{i\alpha}{2}(e^{i\phi} + U_{pq})\right)|0\rangle. \tag{3.9}$$

We then measure the intensity difference between the modes. This is

$$\begin{aligned} I_{\tilde{b}_1} - I_{\tilde{b}_0} &= \langle \hat{\tilde{b}}_1^\dagger \hat{\tilde{b}}_1 - \hat{\tilde{b}}_0^\dagger \hat{\tilde{b}}_0 \rangle \\ &= |\alpha|^2 \,\mathrm{Re}[e^{-i\phi} U_{pq}]. \end{aligned} \tag{3.10}$$

Thus by choosing ϕ as 0 or $\frac{\pi}{2}$, we are able to find the real part and the imaginary part of the matrix element U_{pq} respectively. By choosing $p, q \in 1, 2, ...N$ we can find all the matrix elements in $O(N^2)$ measurements. This completes the characterization of the unitary matrix.

Sensitivity of the scheme

In order to quantify how accurately we can reconstruct the matrix elements by the above-mentioned, scheme, we utilize tools from the theory of quantum metrology. Our aim is to find how the uncertainty in the real and imaginary parts of the matrix element U_{pq} scales with the number of photons used, which in this case is $|\alpha|^2$. For this, in addition to the expectation value of the intensity difference operator that we found in Eq. (3.10), we will find its derivative with the reconstructed matrix elements as well as the variance of this operator.

As found in Eq. (3.10),

$$\begin{aligned}\langle\hat{O}\rangle &\equiv I_{\tilde{b}_1} - I_{\tilde{b}_0} \\ &= \langle\hat{\tilde{b}}_1^\dagger\hat{\tilde{b}}_1 - \hat{\tilde{b}}_0^\dagger\hat{\tilde{b}}_0\rangle \\ &= |\alpha|^2\,\mathrm{Re}[e^{-i\phi}U_{pq}].\end{aligned} \tag{3.11}$$

To find the variance of this operator, we find

$$\langle\hat{O}^2\rangle = \langle\left(\hat{\tilde{b}}_1^\dagger\hat{\tilde{b}}_1 - \hat{\tilde{b}}_0^\dagger\hat{\tilde{b}}_0\right)^2\rangle \tag{3.12}$$

In order to evaluate this, noticing that the output states are coherent states, we proceed to write the operator in normal ordering as

$$\hat{O}^2 = \hat{\tilde{b}}_1^\dagger\hat{\tilde{b}}_1^\dagger\hat{\tilde{b}}_1\hat{\tilde{b}}_1 + \hat{\tilde{b}}_0^\dagger\hat{\tilde{b}}_0^\dagger\hat{\tilde{b}}_0\hat{\tilde{b}}_0 + \hat{\tilde{b}}_1^\dagger\hat{\tilde{b}}_1 + \hat{\tilde{b}}_0^\dagger\hat{\tilde{b}}_0 - 2\hat{\tilde{b}}_1^\dagger\hat{\tilde{b}}_1\hat{\tilde{b}}_0^\dagger\hat{\tilde{b}}_0. \tag{3.13}$$

Evaluating the expectation value of this operator, we obtain

$$\langle\hat{O}^2\rangle = |\alpha|^4\left(\mathrm{Re}[e^{-i\phi}U_{pq}]\right)^2 + \frac{|\alpha|^2}{2}\left(1 + |U_{pq}|^2\right). \tag{3.14}$$

Using Eq. (3.10) and Eq. (3.14), we calculate the standard deviation of the intensity difference operator as

$$\begin{aligned}\Delta\hat{O} &\equiv \langle\hat{O}^2\rangle - \langle\hat{O}\rangle^2 \\ &= \sqrt{\frac{|\alpha|^2}{2}\left(1 + |U_{pq}|^2\right)}.\end{aligned} \tag{3.15}$$

We will now find the derivative of the expectation value of the intensity difference operator with the real and imaginary parts of the matrix elements. When the real part of the matrix element is to be obtained, we fix the phase of the phase-shifter to be zero so that, from

Eq. (3.10), we observe

$$\langle \hat{O} \rangle \overset{\phi=0}{=} |\alpha|^2 \, \mathrm{Re}[U_{pq}] \tag{3.16}$$

Therefore, the derivative of the expectation value of the intensity difference operator with the real part of the matrix elements is

$$\frac{\partial \langle \hat{O} \rangle}{\partial \mathrm{Re}[U_{pq}]} = |\alpha|^2. \tag{3.17}$$

Finally, we calculate the uncertainty in the matrix element obtained as

$$\begin{aligned} \Delta \mathrm{Re}[U_{pq}] &= \frac{\Delta \hat{O}}{\left| \frac{\partial \langle \hat{O} \rangle}{\partial \mathrm{Re}[U_{pq}]} \right|} \\ &= \frac{1}{|\alpha|} \sqrt{\frac{(1 + |U_{pq}|^2)}{2\mathrm{Re}[U_{pq}]^2}} \end{aligned} \tag{3.18}$$

As the total number of photons used is $|\alpha|^2$, our scheme is shot-noise limited.

3.4 Characterization of Bogoliubov transformations

Having seen how unitary evolutions of the mode operators can be characterized, we now move on to characterizing Bogoliubov transformations. In such devices the mode operators evolve as

$$\hat{a}_i^\dagger = U_{ij} \hat{b}_j^\dagger + V_{ij} \hat{b}_j, \tag{3.19}$$

where $UU^\dagger - VV^\dagger = \mathbb{1}$. Note that U here is unitary iff $V = 0$. Hence in general our aim is to find both U and V. We will first find U, and then use that information to find V.

As before, consider a d-mode device where the input and output modes are labeled as a_i and b_i respectively where $i \in \{1, 2, ...N\}$. For finding U, we use a scheme similar to the unitary case but with single photon probes. We first input a single photon in mode $\tilde{a}_0$. The state after the first beam splitter is

$$|\Psi\rangle = \left(\frac{\hat{a}_0^\dagger + i\hat{a}_p^\dagger}{\sqrt{2}} \right) |0\rangle. \tag{3.20}$$

This state is transformed to

$$|\Psi\rangle = \left(\frac{e^{i\phi}\hat{b}_0^\dagger}{\sqrt{2}} + \frac{iU_{pj}\hat{b}_j^\dagger}{\sqrt{2}} \right) |0\rangle, \tag{3.21}$$

where we have noted that $\hat{b}_i|0\rangle = 0 \,\forall\, i$.

The modes b_0 and b_q transform in the beamsplitter so as to yield the final state

$$|\Psi\rangle = \left[\frac{(e^{i\phi} - U_{pq})}{2}\hat{\tilde{b}}_0^\dagger + \frac{(ie^{i\phi} + iU_{pq})}{2}\hat{\tilde{b}}_1^\dagger + \sum_{j\neq q} \frac{iU_{pj}b_j^\dagger}{\sqrt{2}} \right] |0\rangle. \tag{3.22}$$

The difference in the probabilities of measuring the photons at the output of the final beam splitter is

$$P_{\tilde{b}_1} - P_{\tilde{b}_0} = \mathrm{Re}[e^{-i\phi}U_{pq}]. \tag{3.23}$$

As earlier, by choosing ϕ and p, q, we can fully characterize the matrix U.

We now need to characterize V. For this, we send in a coherent state probe as in the unitary case. Proceeding as earlier, we find the reduced state of modes b_0 and b_q as

$$|\tilde{\Psi}\rangle = \hat{\mathcal{D}}_{b_0}\left(\frac{e^{i\phi}\alpha}{\sqrt{2}} \right) \otimes \hat{\mathcal{D}}_{b_q}\left(\frac{i\alpha U_{pq}}{\sqrt{2}} + \frac{i\alpha^* V_{pq}^*}{\sqrt{2}} \right) |0\rangle \ . \tag{3.24}$$

For simplicity, define $\beta_{pq} = \alpha U_{pq} + \alpha^* V_{pq}^*$. After the final beamsplitter, this state is

$$|\tilde{\Psi}\rangle = \hat{\mathcal{D}}_{\tilde{b}_0}\left(\frac{e^{i\phi}\alpha - \beta_{pq}}{2} \right) \otimes \hat{\mathcal{D}}_{\tilde{b}_1}\left(\frac{i(e^{i\phi}\alpha + \beta_{pq})}{2} \right) |0\rangle \ . \tag{3.25}$$

In this case, the intensity difference between the outputs is

$$I_{\tilde{b}_1} - I_{\tilde{b}_0} = \mathrm{Re}[\beta_{pq}\alpha^* \mathrm{e}^{-\mathrm{i}\phi}]. \tag{3.26}$$

This allows us to find $\beta_{pq}\ \forall\, p, q$ which, can be used to find V completely. Note that the above expression reduces to Eq. (3.10) if $V = 0$. This completes the characterization of

Bogoliubov transformations.

3.5 Characterization of Lossy devices

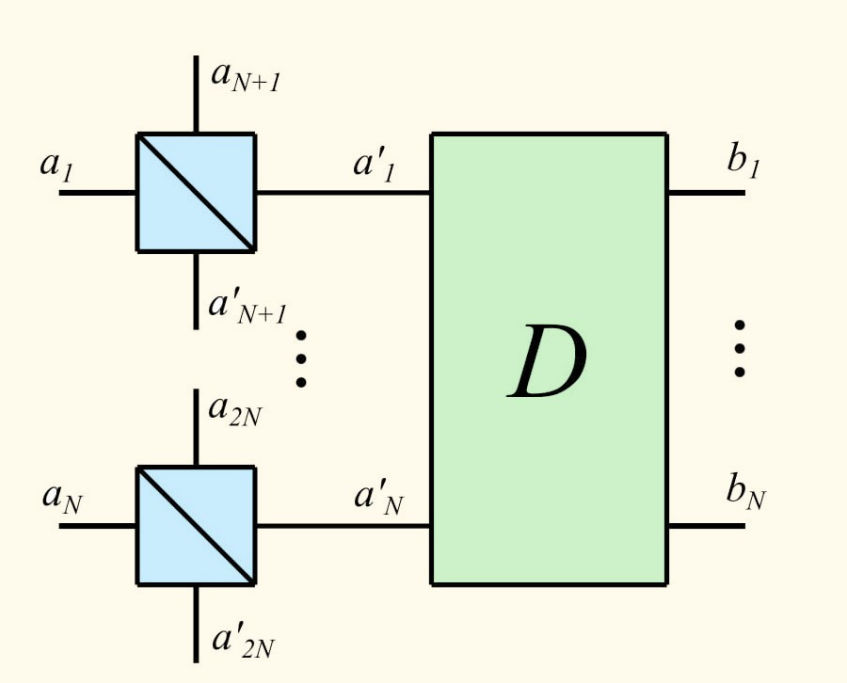

Figure 3.2: The loss of the device is modeled by fictitious beam splitters. The input modes of the beam splitter are labeled a_i and the input modes of the unknown device are labeled a'_i. The auxillary mode of the ith beam splitter introduced which we have no access to is labeled a_{N+i}.

Having discussed how to characterize both unitary and Bogoliubov transformations in lossless devices, we now turn our attention to lossy devices. As shown in Ref. [35], if the loss is independent of the path taken by the photon in the device, then the loss can be modeled by fictitious beam splitters. This embeds the transformation matrices of the device in a larger matrix. Akin to the model in Ref. [35], we attach a fictitious beam splitter of transmissivity $\eta_i \in [0, 1]$ to the i^{th} input mode of the device. This is represented in Fig. 3.2.

The fictitious beam splitters transform the modes as

$$\begin{pmatrix} \hat{a}_i^\dagger \\ \hat{a}_{N+i}^\dagger \end{pmatrix} = \begin{pmatrix} \eta_i & -\sqrt{1-\eta_i^2} \\ \sqrt{1-\eta_i^2} & \eta_i \end{pmatrix} \begin{pmatrix} \hat{a}_i'^\dagger \\ \hat{a}_{N+i}'^\dagger \end{pmatrix} \tag{3.27}$$

where η_i is the transmissivity of the ith beamsplitter. For convenience, define the diagonal

matrices η and $\tilde{\eta}$ as

$$\begin{aligned}\eta_{ij} &= \eta_i \delta_{ij}, \\ \tilde{\eta}_{ij} &= \sqrt{1-\eta_i^2}\delta_{ij}.\end{aligned} \tag{3.28}$$

3.5.1 Unitary transformations

We now focus on the case of a lossy unitary device. In this case, we have

$$\hat{a}_i^{'\dagger} = U_{ij}\hat{b}_j^{\dagger}. \tag{3.29}$$

Combining Eqs. (3.27), (3.28), and (3.29) we obtain

$$\mathbf{a}^{\dagger} = \mathbf{U}\mathbf{b}^{\dagger}, \tag{3.30}$$

where

$$\mathbf{a}^{\dagger} = (a_1^{\dagger}...a_{2N}^{\dagger})^T, \tag{3.31}$$

$$\mathbf{b}^{\dagger} = (b_1^{\dagger}...b_N^{\dagger}, \hat{a}_{N+1}^{'\dagger}...\hat{a}_{2N}^{'\dagger})^T, \tag{3.32}$$

and

$$\mathbf{U} = \begin{pmatrix} (\eta U)_{N\times N} & (-\tilde{\eta}\mathbb{1})_{N\times N} \\ (\tilde{\eta}U)_{N\times N} & (\eta\mathbb{1})_{N\times N} \end{pmatrix}. \tag{3.33}$$

It is this $2N \times 2N$ matrix that now characterizes the device. Thus, in addition to U, we need to find η and $\tilde{\eta}$. In order to find the losses, we send in a coherent state into mode a_i. The state evolves as

$$\begin{aligned}|\Psi\rangle = \hat{\mathcal{D}}_{a_i}(\alpha)|0\rangle &= \hat{\mathcal{D}}_{a_i'}(\eta_i\alpha) \otimes \hat{\mathcal{D}}_{a'_{N+i}}(-\sqrt{1-\eta_i^2}\alpha)|0\rangle, \\ &= \otimes_{j=1}^{N}\hat{\mathcal{D}}_{b_j}(\eta_i U_{ij}\alpha) \otimes \hat{\mathcal{D}}_{a'_{N+i}}(-\sqrt{1-\eta_i^2}\alpha)|0\rangle.\end{aligned} \tag{3.34}$$

Then the sum of the intensities in the accessible output modes is

$$I = \eta_i^2 \sum_j |U_{ij}|^2 |\alpha|^2 = \eta_i^2 |\alpha|^2. \tag{3.35}$$

From this, all η_i and hence η and $\tilde{\eta}$ can be found out. In order to find U, we proceed exactly as in the lossless unitary case. We will see that Eq. (3.10) will be modified to read

$$I_{\tilde{b}_1} - I_{\tilde{b}_0} = |\alpha|^2 \, \mathrm{Re}[e^{-i\phi} \eta_p U_{pq}], \tag{3.36}$$

from which we can now find U. Thus the lossy unitary device can be characterized.

3.5.2 Bogoliubov transformations

We now move on to lossy devices that implement Bogoliubov transformations. In such devices, the mode operators evolve as

$$\hat{a}_i^{'\dagger} = U_{ij} \hat{b}_j^{\dagger} + V_{ij} \hat{b}_j. \tag{3.37}$$

Modeling the loss as earlier, the full transformation becomes

$$\mathbf{a}^{\dagger} = \mathbf{U}\mathbf{b}^{\dagger} + \mathbf{V}\mathbf{b}, \tag{3.38}$$

where $\mathbf{a}^{\dagger}$, $\mathbf{b}^{\dagger}$, and $\mathbf{U}$ are defined in Eqs. 3.31, 3.32, and 3.33, and

$$\mathbf{V} = \begin{pmatrix} (\eta V)_{N\times N} & \mathbb{0}_{N\times N} \\ (\tilde{\eta} V)_{N\times N} & \mathbb{0}_{N\times N} \end{pmatrix}. \tag{3.39}$$

Thus we have to find U, V, η, and $\tilde{\eta}$ in order to fully characterize this device. In order to find η we send in a single photon in mode a_i. The probability that the photon will be detected in any of the accessible output modes in $|\eta_i|^2$. Thus η and $\tilde{\eta}$ can be found out. To find U, we proceed exactly as in the case of lossless Bogoliubov transformations so that

Eq. (3.23) will be modified to

$$P_{\tilde{b}_1} - P_{\tilde{b}_0} = \mathrm{Re}[e^{-i\phi}\eta_p U_{pq}], \tag{3.40}$$

from which U can be found. Similarly, Eq. (3.26) will be modified to

$$P_{\tilde{b}_1} - P_{\tilde{b}_0} = \mathrm{Re}[e^{-i\phi}\alpha^*\eta_p\beta_{pq}], \tag{3.41}$$

which enable us to find V. This completes the characterization of lossy Bogoliubov transformations.

3.6 Characterization of unitary transformations with coherent light and squeezed vacuum

In Sec. 2.6, we have seen that when coherent light and squeezed vacuum are used as inputs to a Mach-Zehnder interferometer, then the precision of phase estimation beats the standard shot-noise limit. It is natural then to see if the same states of light can be used as inputs for a modified Mach-Zehnder interferometer in order to characterize a linear optical system below the shot-noise limit. For simplicity, we will restrict our attention to a two-mode linear optical device as shown in Fig. 3.3. As coherent states as well as squeezed vacuum are Gaussian states, and as we evolve it through a linear optical device, we will use the tools of Gaussian quantum information to describe this system.

3.6.1 Description of the evolution

We will first see how the covariance matrix describing the quantum state evolves via the modified Mach-Zehnder interferometer.

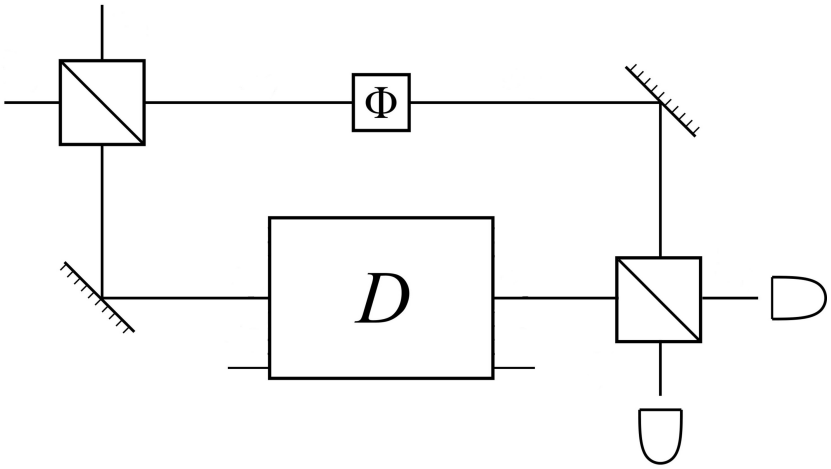

Figure 3.3: Modified Mach-Zehnder interferometer with coherent and squeezed vacuum inputs for characterizing a two-mode unitary device. The upper input an output modes of the unitary are connected to the lower arm of the interferometer.

Initially, the covariance matrix of the input is given as

$$S = \begin{pmatrix} 1 & 0 & 0 & 0 \\ 0 & e^{-2r} & 0 & 0 \\ 0 & 0 & 1 & 0 \\ 0 & 0 & 0 & e^{2r} \end{pmatrix} \tag{3.42}$$

After the first beamsplitter, the covariance matrix is

$$V \xrightarrow{BS} \frac{1}{2} \begin{pmatrix} 1+e^{2r} & 0 & 0 & -1+e^{2r} \\ 0 & 1+e^{-2r} & 1-e^{-2r} & 0 \\ 0 & 1-e^{-2r} & 1+e^{-2r} & 0 \\ -1+e^{2r} & 0 & 0 & 1+e^{2r} \end{pmatrix} \tag{3.43}$$

Subsequently, the upper arm of the interferometer evolves through a phase-shifter while

the lower arm consists of the first input and the first output ports of the unitary device. This evolution is characterized by the evolution matrix

$$S_{\Phi,\mathbf{U}} = \begin{pmatrix} \cos(\phi) & 0 & 0 & -\sin(\phi) & 0 & 0 \\ 0 & \mathrm{Re}(U_{11}) & \mathrm{Re}(U_{12}) & 0 & -\mathrm{Im}(U_{11}) & -\mathrm{Im}(U_{12}) \\ 0 & \mathrm{Re}(U_{21}) & \mathrm{Re}(U_{22}) & 0 & -\mathrm{Im}(U_{21}) & -\mathrm{Im}(U_{22}) \\ \sin(\phi) & 0 & 0 & \cos(\phi) & 0 & 0 \\ 0 & \mathrm{Im}(U_{11}) & \mathrm{Im}(U_{12}) & 0 & \mathrm{Re}(U_{11}) & \mathrm{Re}(U_{12}) \\ 0 & \mathrm{Im}(U_{21}) & \mathrm{Im}(U_{22}) & 0 & \mathrm{Re}(U_{21}) & \mathrm{Re}(U_{22}) \end{pmatrix}. \tag{3.44}$$

However, this is the evolution matrix for a three mode system. Noting that the lower port of the unitary device is also fed in vacuum, we modify the covariance matrix in Eq. (3.43) so as to obtain the covariance matrix of a three mode system. Then covariance matrix further evolves as

$$V \xrightarrow{\Phi,\mathbf{U}} S_{\Phi,\mathbf{U}}\, V\, S^{T}_{\Phi,\mathbf{U}}. \tag{3.45}$$

The lower modes of system are traced out, and interact with a beamsplitter again. The final covariance matrix is given in Appendix A.

Similarly, we can find the evolution of the mean vector. Without loss of generality let us assume that the amplitude of the coherent state is real. The initial mean vector of the system is

$$\bar{\mathbf{x}} = \begin{pmatrix} 2\alpha \\ 0 \\ 0 \\ 0 \end{pmatrix}. \tag{3.46}$$

The mean vector evolves as per Eq. (2.73) so that the final mean vector is given as

$$\bar{\mathbf{x}} = \alpha \begin{pmatrix} \cos(\phi) - \mathrm{Re}(U_{11}) \\ \mathrm{Im}(U_{11}) + \sin(\phi) \\ \sin(\phi) - \mathrm{Im}(U_{11}) \\ -\mathrm{Re}(U_{11}) - \cos(\phi) \end{pmatrix} \tag{3.47}$$

Having obtained the covariance matrix and the mean vector, we calculate the expectation value of the intensity difference operator as

$$\langle \hat{I}_a - \hat{I}_b \rangle = -\left(\alpha^2 + \sinh^2(r)\right)\left(\mathrm{Re}(e^{-i\phi}U_{11})\right). \tag{3.48}$$

Thus by choosing $\phi = 0, \frac{\pi}{2}$ we can obtain the real and imaginary parts of the matrix element respectively. We also note that the expectation value of the intensity difference is proportional to the mean number of photons $\bar{n}$.

In order to find the sensitivity of this scheme, we find the variance of the intensity difference operator. As this expression contains the fourth moments of mode operators, we employ the Wick's theorem to reduce it to products of the first and second moments of the quadrature operators. As the first and second moments are given by the covariance matrix and the mean vector, we obtain the variance of the intensity difference as

$$\begin{aligned} \langle \Delta^2 I \rangle = \frac{1}{8}\Big[& |U_{11}|^2(-1 + 4\alpha^2\cosh 2r + \cosh 4r) + 4(\alpha^2 + \sinh^2 r) \\ & + 4\sinh^2(r)(2\alpha^2 + \cosh 2r)\mathrm{Re}\left(e^{-2i\phi}U_{11}^2\right)\Big] \end{aligned} \tag{3.49}$$

This variance is minimized when $|U_{11}|^2 \to 0$. Under this assumption, the variance in Eq. (3.49) is proportional to the mean number of photons input $\bar{n}$. We now find the sensitivity of our scheme using the error propagation formula in Eq. (2.88).

We observe that the sensitivity of this scheme is also limited by the shot-noise limit

even though we have coherent and squeezed vacuum inputs. This is hypothesized to be an effect of the fact that the unmeasured ports of the unitary device has vacuum inputs. It was found in Ref. [46] that a Mach-Zehnder interferometer is limited by shot noise when at least one of the inputs is vacuum. We suspect this might indeed be the case here.

3.7 Summary

In this chapter we have seen that a modified Mach-Zehnder interferometer can characterize both unitary and Bogoliubov transformations. We have modeled loss in our devices using fictitious beamsplitters. We have also demonstrated that the sensitivity of this scheme is limited by shot noise.

Chapter 4
Characterizing Photodetectors via Wigner functions

In this chapter I will develop a scheme to characterize photodetectors. This is done by developing a scheme to find the Wigner functions of the POVM elements corresponding to a detector. After motivating this work, I will discuss a method to find the Wigner functions of the POVM elements from experimental data. I will then show a schematic of the experimental setup required. I will show how prior knowledge of the characteristics of the detector helps us to drastically reduce the resource requirements of this scheme. Finally, I will use methods from convex quadratic optimization to make this reconstruction robust to experimental noise. [1]

4.1 Introduction

Photodetection has been making consistent progress with rapidly developing optical quantum technology [47, 48, 49, 50, 51, 52]. In addition to being an integral part of quantum technology such as quantum computing [31], quantum enhanced metrology [16], and quantum communication [53], photodetectors also play a key role in probing the foundations of physics [54].

As mentioned in Sec. 2.4, every quantum detector is fully characterized by a set of positive semi-definite measurement operators $\{M_k\}$ called as Positive Operator Valued Measures (POVMs). When a quantum detector measures a quantum state $\hat{\rho}$, the probability of observing an outcome k is

$$p(k)_\rho = \mathrm{Tr}[\hat{\rho}\hat{M}_k]. \tag{4.1}$$

In order to identify the POVM elements of a detector, one can invert Eq. (4.1) which is known as Quantum Detector Tomography (QDT). In optical QDT, light prepared in a set of known tomographically complete states — referred to as probes — is incident on the detector to be characterized. The probabilities of different measurement outcomes is then

[1] This chapter is based on Rajveer Nehra and Kevin Valson Jacob, arXiv 1909.10628.

used to characterize the detector.

One such possible set of probes is composed of coherent states $\{|\alpha\rangle\langle\alpha|\}$. With a coherent state $|\alpha\rangle$ as the probe, the probability of outcome k is given as

$$p(k)_{|\alpha\rangle} = \mathrm{Tr}\left[|\alpha\rangle\langle\alpha|M_k\right] = \pi Q_{M_k}(\alpha), \tag{4.2}$$

where $Q_{M_k}(\alpha)$ is the Husimi Q quasi-probability distribution corresponding to the detector POVM element M_k. Therefore, one can reconstruct the Q functions for POVM elements directly from the measurement statistics, and thereby fully characterize the detector.

From knowing the Q distribution of all POVM elements of a detector, one can predict the measurement outcomes for an arbitrary quantum state using its Glauber–Sudarshan P representation. Consider a quantum state ρ represented as

$$\rho = \int P_\rho(\alpha)|\alpha\rangle\langle\alpha|\, d^2\alpha, \tag{4.3}$$

where $d^2\alpha := d\mathrm{Re}(\alpha)d\mathrm{Im}(\alpha)$. The probability of outcome k can then be obtained using the Born rule as

$$p(k)_\rho = \mathrm{Tr}[\rho M_k] = \pi \int P_\rho(\alpha) Q_{M_k}(\alpha) d^2\alpha. \tag{4.4}$$

Therefore, by using the Q representation for detector POVM elements and P representation for the input quantum state, one can, in principle determine the outcome probabilities corresponding to detector outcomes.

However, this approach suffers from an inherent shortcoming due to the highly singular nature of P functions for non-classical states of the optical field [5]. In addition, as discussed in [55], experimental errors and statistical noise during the experiments may distort Q functions resulting in nonphysical POVM elements. In order to alleviate these problems, I develop a method to characterize the quantum detector by experimentally obtaining the Wigner functions of the POVM elements of the detector. By obtaining the Wigner functions

of the detector, any experimental probability can be found in terms of the Wigner functions of the state as well as of the detector, which are well-behaved unlike P functions. Thus, the Born rule can be rewritten as

$$p(k)_\rho = \mathrm{Tr}[\rho M_k] = \pi \int W_\rho(\alpha) W_{M_k}(\alpha)\, d^2\alpha, \tag{4.5}$$

where $W_\rho(\alpha)$ and $W_{M_k}(\alpha)$ are the Wigner functions of quantum state ρ and POVM element M_k respectively.

4.2 Method

We use the well known result that the Wigner function operator can be represented in Fock space as

$$\hat{W}(\alpha) = \frac{2}{\pi} \sum_{n=0}^{\infty} (-1)^n \hat{D}(\alpha)|n\rangle\langle n|\hat{D}^\dagger(\alpha), \tag{4.6}$$

where $\hat{D}(\alpha) = \exp\big(\alpha\hat{a}^\dagger - \alpha^*\hat{a}\big)$ is the displacement operator with $\alpha \in \mathbb{C}$. The Wigner function of any positive semi-definite operator $\hat{O}$ can then be found as

$$W_{\hat{O}}(\alpha) = \mathrm{Tr}[\hat{O}\hat{W}(\alpha)]. \tag{4.7}$$

In particular, the Wigner function of a POVM element M_k can then be written as

$$W_{M_k}(\alpha) = \frac{2}{\pi} \sum_{n=0}^{\infty} (-1)^n \mathrm{Tr}\left[M_k \hat{D}(\alpha)|n\rangle\langle n|\hat{D}^\dagger(\alpha)\right]. \tag{4.8}$$

For simplicity in notation, we define

$$P^{(n)}_{M_k}(\alpha) := \mathrm{Tr}\left[M_k \hat{D}(\alpha)|n\rangle\langle n|\hat{D}^\dagger(\alpha)\right]. \tag{4.9}$$

The function $P^{(n)}_{M_k}(\alpha)$ represents the probability of outcome k when the Fock state $|n\rangle$, after being displaced by α, interacts with the detector.

Although the summation in Eq. (4.8) has infinite terms, for many POVM elements,

latter terms don't significantly contribute to the sum. Therefore, one can truncate the summation as

$$W_{M_k}(\alpha) \approx \frac{2}{\pi} \sum_{n=0}^{n_0} (-1)^n P_{M_k}^{(n)}(\alpha), \tag{4.10}$$

where we only consider the first $n_0 + 1$ terms of the summation. From Eq. (4.10) we can see that finding the Wigner function corresponding to the POVM element M_k amounts to finding out all these summands.

In this chapter, I will restrict ourselves to phase-insensitive detectors for simplicity. Such detectors have the Wigner functions of their POVM elements rotationally symmetric around the origin, and hence can be characterized on the real line alone. However, we note that this scheme is applicable to phase-sensitive detectors also; and for such detectors, we have to choose α in the complex plane.

4.2.1 Proposed experimental setup

Fig. 4.1 shows a schematic for our proposed experiment. A laser beam is split into two beams at the first beamsplitter (BS). One beam is used to generate thermal states. Thermal states can be generated by randomzing the phase and amplitude of the laser beam (coherent state). To achieve that, we use a Variable Neutral Density Filter (VNDF) along with a Rotating Ground-Glass Disk (RGGD). VNDF allows to produce coherent states of variable amplitudes, which are further fed to RGGD for the phase and amplitude randomization in order to produce thermal states [56]. The other beam is used as a Local Oscillator (LO) whose amplitude and phase are modulated to reconstruct the Wigner functions over the entire phase space. Amplitude and phase modulation is achieved using Local Oscillator Modulator (LOMD). For phase space displacement implementation, we interfere thermal states with the LO at a highly unbalanced beamsplitter denoted as DBS in the experiment schematic.

In order to characterize the detector, we consider $(n_0 + 1)$ distinct thermal states given

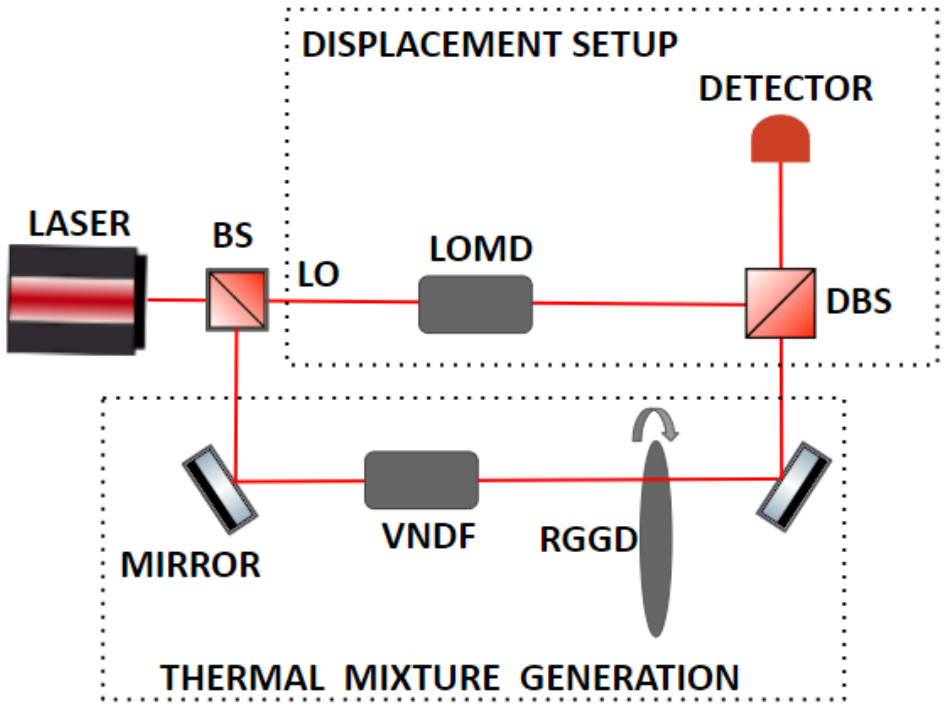

Figure 4.1: Schematic of the experimental setup. BS: beamsplitter. LO: Local Oscillator. VNDF: Variable Neutral Density Filter. RGGD: Rotating Ground-Glass Disk. DBS: Displacement beamsplitter. LOMD: Local oscillator modulator.

as

$$\rho^{(j)} = \sum_{n=0}^{\infty} p_n^{(j)} \, |n\rangle\langle n| \tag{4.11}$$

where $j = 0, \ldots, n_0$ labels the thermal states, and

$$p_n^{(j)} = \frac{\bar{n}_j^n}{(1+\bar{n}_j)^{n+1}} \tag{4.12}$$

is the Bose-Einstein photon-number distribution of a thermal state $\rho^{(j)}$ with mean photon-number $\bar{n}_j$. We then displace these thermal states by amplitude α which is, for phase insensitive detectors, chosen to be real. Then, the probability of obtaining k outcome with the displaced thermal input as input is give by

$$R_k^{(j)}(\alpha) \approx \sum_{n=0}^{n_0} p_n^{(j)} P_{M_k}^{(n)}(\alpha), \tag{4.13}$$

where we choose the thermal states such that the contribution to the RHS from the omitted terms is negligible. This is possible because the thermal state has an exponentially decreasing photon number distribution. In matrix form, we can write Eq. (4.13) as

$$\begin{pmatrix} R_k^{(0)}(\alpha) \\ R_k^{(1)}(\alpha) \\ \vdots \\ R_k^{(n_0)}(\alpha) \end{pmatrix} = \begin{pmatrix} p_0^{(0)} & p_1^{(0)} & \dots & p_{n_0}^{(0)} \\ p_0^{(1)} & p_1^{(1)} & \dots & p_{n_0}^{(1)} \\ \vdots & & & \\ p_0^{(n_0)} & p_1^{(n_0)} & \dots & p_{n_0}^{(n_0)} \end{pmatrix} \begin{pmatrix} P_{M_k}^{(0)}(\alpha) \\ P_{M_k}^{(1)}(\alpha) \\ \vdots \\ P_{M_k}^{(n_0)}(\alpha) \end{pmatrix}. \tag{4.14}$$

We can further write Eq. (4.14) compactly as

$$\mathbf{R} = \mathbf{P}\mathbf{\Pi}^{\alpha}_{\mathbf{M_k}}, \tag{4.15}$$

where $\mathbf{R}$ and $\mathbf{\Pi}^{\alpha}_{\mathbf{M_k}}$ are vectors of length (n_0+1), and $\mathbf{P}$ is the probability distribution square matrix of dimension $(n_0+1)\times(n_0+1)$. Thus by solving Eq. (4.15), we can determine $\mathbf{\Pi}^{\alpha}_{\mathbf{M_k}}$, which allows us to calculate the summation in Eq. (4.8).

To solve for $\mathbf{\Pi}^{\alpha}_{\mathbf{M_k}}$, one needs to solve the following convex quadratic optimization problem:

$$\begin{aligned} &\text{Minimize } \left|\left|\mathbf{R} - \mathbf{P}\mathbf{\Pi}^{\alpha}_{\mathbf{M_k}}\right|\right|_2, \\ &\text{Subject to } 0 \le \mathbf{\Pi}^{\alpha}_{\mathbf{M_k}} \le 1, \\ &\qquad -1 \le \sum_{n=0}^{n_0} (-1)^n P_{M_k}^{(n)}(\alpha) \le 1, \end{aligned} \tag{4.16}$$

where $\|.\|$ is the l_2 norm defined for a vector V as

$$\|V\|_2 = \left(\sum_i |V_i|^2\right)^{\frac{1}{2}}. \tag{4.17}$$

The optimization constraints in Eq. (4.16) can be understood as follows:

The first constraint follows from the fact that the n^{th} element $P^{(n)}_{M_k}(\alpha)$ of $\mathbf{\Pi^{\alpha}_{M_k}}$ is the probability of getting outcome k if a displaced n-photon Fock state is incident to the detector. Therefore, we have $0 \leq P^{(n)}_{M_k}(\alpha) \leq 1$.

The second constraint follows from the fact that Wigner functions are well-defined and bounded between $[-2/\pi, 2/\pi]$ for a POVM element corresponding to a phase-insensitive detector. This is because the POVM element in such a case is a statistical mixture of projectors.

Solving this optimization problem in Eq. (4.16) allows us to determine the Wigner function at a given phase space point α. Further, we can repeat the process with different displacement amplitudes to reconstruct the Wigner function over the entire phase space. In practice, the Wigner functions of various detectors are localized around the origin and vanishes to zero for large α, so it is unnecessary to displace the thermal states with arbitrarily large α.

In the following section we numerically simulate this method for a phase-insensitive detector. We hasten to add that this method is applicable to any type of detector.

4.3 Modelling a Photon-number-resolving detector

In this section, we reconstruct the Wigner functions of a perfect and an imperfect photon-number-resolving (PNR) detector. In general, a POVM element corresponding to 'k' outcome can be written in the photon-number basis as

$$M_k = \sum_{m,n=0}^{\infty} \langle m|M_k|n\rangle |m\rangle\langle n|, \tag{4.18}$$

where $\langle m|M_k|n\rangle$ are the matrix elements of the POVM operator. One can further simplify Eq. (4.18) for a PNR detector with no dark counts as

$$M_k = \sum_{m=k}^{m_0} \langle m|M_k|m\rangle |m\rangle\langle m|. \tag{4.19}$$

Note that Eq. (4.19) differs from Eq. (4.18) in three ways. First, the POVM is diagonal

with entries $\langle m|M_k|m\rangle$, which are essentially the probabilities of detecting k photons given m photons are incident to the detector. Thus for a detector with detection efficiency η, we have

$$p(k|m) = \langle m|M_k|m\rangle = \binom{m}{k}\eta^k(1-\eta)^{m-k}. \tag{4.20}$$

Second, we have truncated the sum to m_0 such that it exceeds the photon-number at which saturates the detector. Third, the sum is starting from k because with no dark counts noise, one would expect k clicks only if there are $m \geq k$ photons are incident on the detector.

Eq. (4.19) and Eq. (4.20) can be interpreted as follows: The POVM elements of a perfect PNR detector are projectors $\Pi_m = |m\rangle\langle m|$. However, for an imperfect detector, its efficiency $\eta < 1$. If m photons impinge on such a detector, due to its non-unity detection efficiency, $k < m$ photons results in a detection event contributing a factor of η^k to the probability of the event; while $(m-k)$ photons remain undetected contributing a factor of $(1-\eta)^{m-k}$ to the probability of the event. Thus, such POVMs are statistical mixtures of projective measurements.

In numerical simulations, we considered equidistant 51 displacement amplitudes in $\alpha \in [-3.6, 3.6]$, which allowed us to probe the Wigner function uniformly over the entire region of phase space where the Wigner function is non-vanishing. We used 50 equally spaced thermal states of mean photon-number in $\bar{n} \in [0, 4]$. For all of our simulations in open source Python module QuTip [57], we generally limited the dimension of the Hilbert space to 50, and the sum in Eq. (4.19) was truncated with $m_0 = 50$ at which point $P(k|m_0)$ was of the order of 10^{-10} for $\eta = 0.90$.

In Fig. 4.2, we plot the Wigner functions of one, two, and three photon detections for a perfect detector and an imperfect detector with imperfections as modelled in Eq. (4.19). From Fig. 4.2, we notice that the extrema of the Wigner functions of imperfect detectors are closer to the origin than those of perfect detectors. This is due to the contribution of higher order projectors in the Wigner functions of imperfect detectors. In particular for the imperfect single-photon detection event, we see a reduced negativity in the Wigner

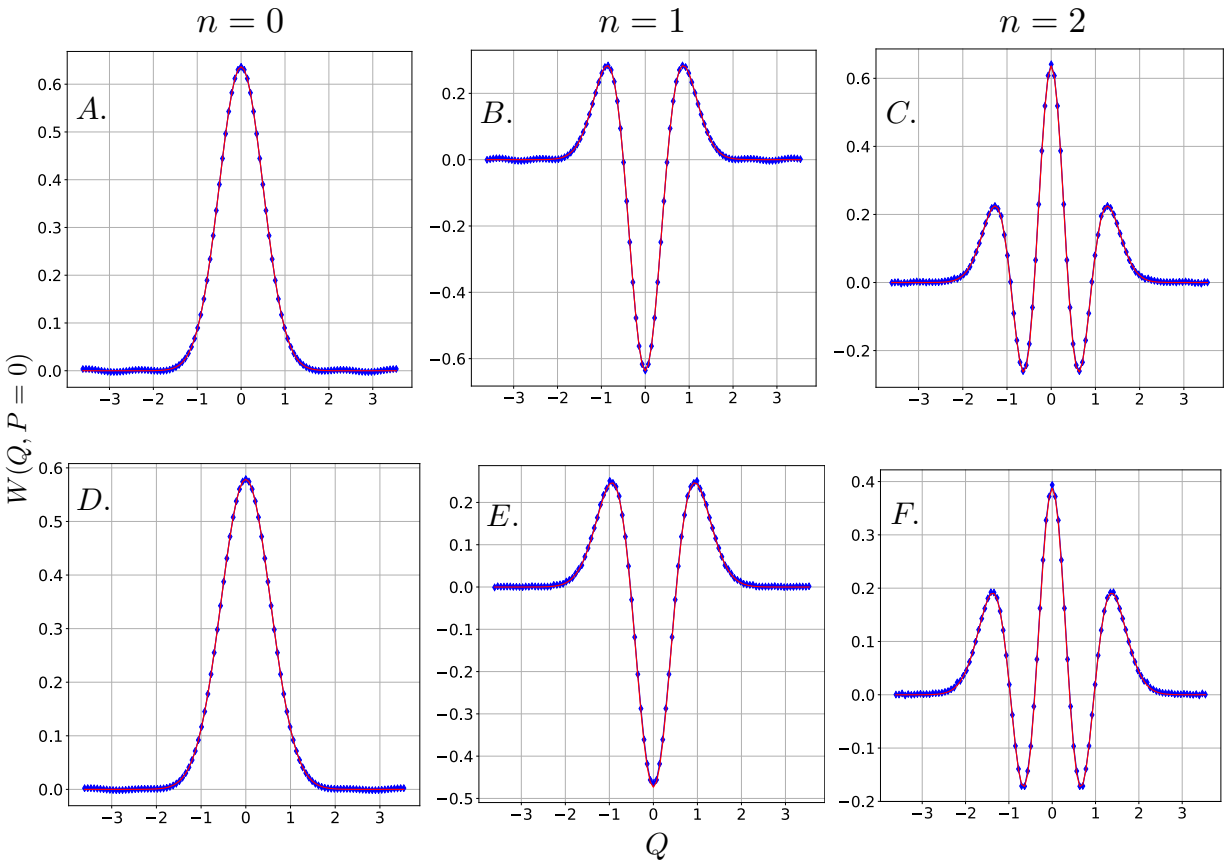

Figure 4.2: Wigner functions for POVM elements corresponding to zero-, one-, and two-photon detection events. Red curves are theoretically expected Wigner functions and blue ones the reconstructed one using the proposed method. In the top row, A, B, and C are for a perfect PNR detector; and in the bottom row, D, E, and F are for a PNR detector with detection efficiency $\eta = 0.90$.

function around the origin. This is due to the contribution of the Wigner function of the two-photon detection event which is strongly positive around origin. Similar arguments can be made for the the reduced positivity of the Wigner function for zero- and two-photon detection event POVMs.

In our reconstruction, we have uniformly sampled the phase space. A natural question that now arises is whether the number of points that needs to be probed in the phase space can be reduced. We investigate this question in the following section.

4.4 Characterizing phase-insensitive detectors with polynomial resources

Although the method outline earlier is general, it had substantial resource requirements as we had to uniformly sample over the phase space. However, this requirement can be drastically reduced if we have the prior knowledge that the detector is phase-insensitive, i.e. the representations of its POVM elements are diagonal in the Fock basis. Note that the phase sensitivity of a detector can easily be checked by varying the phase of the LO while keeping the amplitude fixed. In this case, unlike a PNR detector, a phase sensitive detector outputs different measurement statistics for different phases and fixed amplitudes of the LO.

We recall that the Wigner functions of Fock states are Gaussian modulated Laguerre polynomials. This allows us to write the Wigner function the POVM elememt 'M_k' of a PNR detector as

$$W_{M_k}(\alpha) = \frac{2e^{-2|\alpha|^2}}{\pi} \sum_{m=0}^{m_0} (-1)^m p(k|m)\ \mathcal{L}_m(4|\alpha|^2), \tag{4.21}$$

where $\mathcal{L}_m(x)$ represents the Laguerre polynomial of m^{th} degree in $|\alpha|^2$. As the Wigner function is a function of $|\alpha|^2$, it is symmetric around the origin, and can be fully characterized on the real line. Since the Wigner function is a Gaussian modulated polynomial, the problem of reconstructing it is reduced to finding out a polynomial of degree $2m_0$ in α which requires us to find the Wigner function only at $2m_0 + 1$ points.

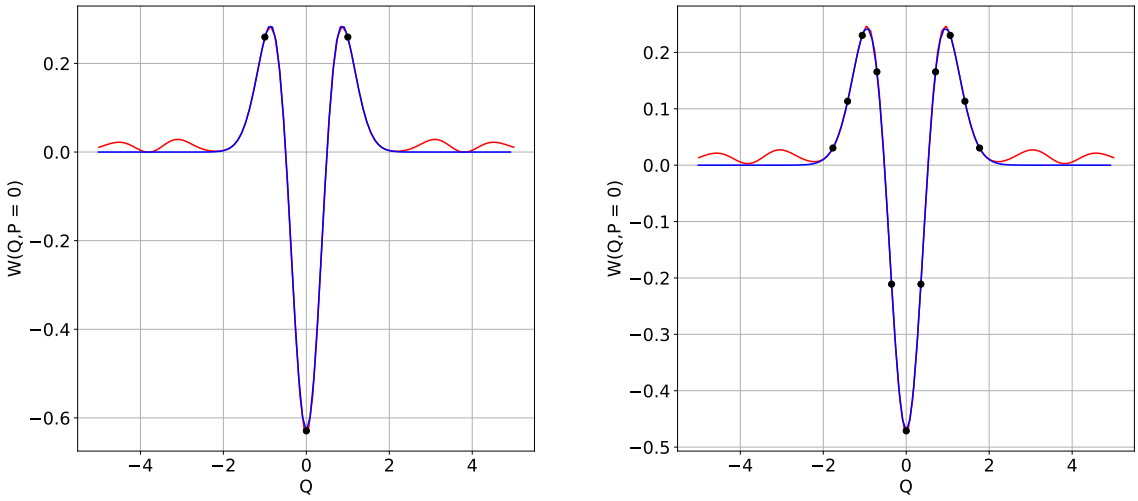

Figure 4.3: Left : Wigner function corresponding to a perfect single-photon detection POVM determined by naive summation up to 15 terms of Eq. (4.8) (Red), and using an Gaussian modulated quadratic fit near the origin (Blue). Black points represent the phase space points where the Wigner function was probed by the proposed method here. The latter approximates well the actual Wigner function. Right : Wigner function corresponding to an imperfect single-photon detection POVM with $\eta = 0.90$.

As an example, we considered the POVM element corresponding to a single-photon detection event for both perfect and imperfect PNR detectors. In Fig. 4.3, the red curves show the POVM determined by the naive summation up to 15 terms of Eq. (4.8); and the blue curves the reconstructed Wigner functions with black points being the phase space coordinates where the Wigner function was probed.

We see that one needs to probe the Wigner function only at three points for a perfect detector because the Laguerre polynomial $\mathcal{L}_{m=1}(4|\alpha|^2)$ is quadratic in α, and therefore can be fully characterized using three distinct points. Likewise, the Wigner function for an imperfect single-photon POVM can be reconstructed using only 11 distinct points (black points in Fig. 4.3) if we truncate the sum in Eq. (4.19) at $m_0 = 5$ where $p(k|m)$ is of the order of 10^{-6}. In this case, we will have to reconstruct an Gaussian modulated polynomials of degree 10 because the last term in the Eq. (4.19) would be a projector, $|5\rangle\langle 5|$ with Wigner function given by Gaussian modulation of $\mathcal{L}_{m=5}(4|\alpha|^2)$.

Note that finding the Gaussian-modulated polynomial also works for a general detector given by Eq. (4.18). However, instead of reconstructing the Wigner function on the real line, we will have to reconstruct it in the complex plane for which appropriate polynomial interpolation schemes have to be used [58].

4.5 Robustness against experimental noise

In this section, we discuss the robustness of this method against experimental noise. In general, inverting Eq. (4.15) is ill-conditioned as seen by the large ratio of the largest and smallest singular values of the matrix $\mathbf{P}$. This makes the reconstructed POVM elements extremely sensitive to small fluctuations in the measurement statistics, and can lead to nonphysical POVMs.

However, the effects of ill-conditioning can be remarkably suppressed by adding a regularization to the optimization problem. Several types of regularization techniques are discussed in detail in [55], and for this work we use Tikhonov regularization [59]. Using this technique, inverting Eq. (4.15) can be mathematically formulated as the following optimization problem:

$$\begin{aligned} &\text{Minimize } \left|\left|\mathbf{R} - \mathbf{P}\mathbf{\Pi}^{\alpha}_{\mathbf{M_k}}\right|\right|_2 + \gamma \left|\left|\mathbf{\Pi}^{\alpha}_{\mathbf{M_k}}\right|\right|_2, \\ &\text{Subject to } 0 \leq \mathbf{\Pi}^{\alpha}_{\mathbf{M_k}} \leq 1, \\ &\qquad -1 \leq \sum_{n=0}^{n_0} (-1)^n P^{(n)}_{M_k}(\alpha) \leq 1, \end{aligned} \tag{4.22}$$

where γ is the regularization parameter. Solving this problem translates to a convex quadratic optimization which can be efficiently solved using a semi-definite problem solver, for instance, the Python package CVXOPT [60].

In order to simulate the presence of noise in our reconstruction, we introduce noise in the LO's amplitude $|\alpha|$. We model this noise as a Gaussian distribution of mean zero and standard deviation $\sigma = 0.01|\alpha|^2$. This is the typical noise level present in currently available stabilized lasers. Therefore, the displacement amplitudes are $(\alpha_1 + \delta d_1, \alpha_2 + \delta d_2 \ldots, \alpha_{max} +$

δd_{max}), where each δd_i is a random variable sampled from the Gaussian distribution. To further reduce the effects of the fluctuations, we average the Wigner functions obtained over $N = 40$ iterations of the optimization. As a result, we get

Having obtained $\overline{W}_{M_k}(\alpha)$, we then we utilize robust nonlinear regression methods to further suppress the fluctuations. We recall that for a phase insensitive detector, the POVMs are Gaussian modulated polynomials of degree $2m_0$ in α, where m_0 is the saturation limit given in Eq. (4.21). Therefore, once we have experimentally probed the Wigner function at $2m_0 + 1$ distinct points of the phase space, we could simply fit a Gaussian modulated polynomial of degree $2m_0$ in α to reconstruct the Wigner function over the entire phase space. Keeping that in mind, we set an optimization problem as:

Minimize:

$$\left\{ \frac{1}{2} \sum_{i=1} L \left[\left(e^{-2|\alpha_i|^2} \text{Poly}(2m_0, \alpha_i) - \overline{W}_{M_k}(\alpha_i) \right)^2 \right] \right\},$$

where L is defined as

$$L(y) = 2(\sqrt{1+y} - 1), \tag{4.23}$$

and $\text{Poly}(2m_0, \alpha_i)$ is a polynomial of degree $2m_0$. Note that this approach of finding the Gaussian modulated polynomial has an advantage of not being biased unlike the simple least-square fitting method which tends to significantly bias in order to avoid high residuals in the data [61].

$$\overline{W}_{M_k}(\alpha) = \frac{\sum_{j=1}^{N} W_{M_k}^{j}(\alpha + \delta\alpha_j)}{N}. \tag{4.24}$$

We further evaluate the quality of reconstruction method by using the relative error defined with l_2 norm as:

$$\triangle := \frac{||W_{M_k}^{\text{theory}}(\alpha) - W_{M_k}^{\text{reconstruted}}(\alpha)||_2}{||W_{M_k}^{\text{theory}}(\alpha)||_2}. \tag{4.25}$$

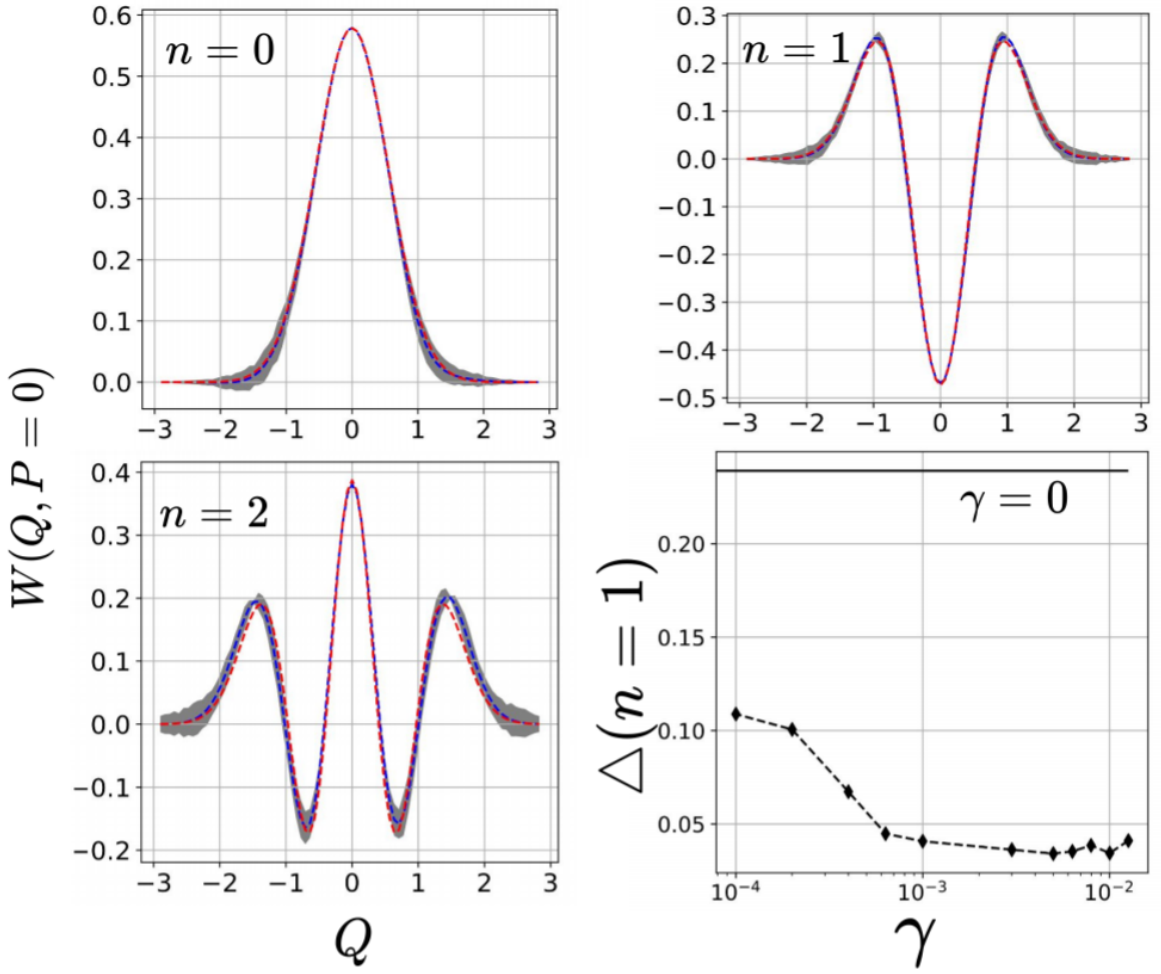

Figure 4.4: Blue: Reconstructed Wigner functions using regularization for zero-,one- and two-photon detection events of a detector with $\eta = 0.90$. Red curves are theoretically expected Wigner functions. Gray areas are error (1σ) obtained using $N = 40$ iterations. Bottom right: Dashed-diamond curve illustrates the robustness of the reconstruction against regularization parameter γ and black solid line is without regularization, i.e, $\gamma = 0$.

The result of our reconstruction is shown in Fig. 4.4. Since the fluctuations grow with increasing local oscillator amplitude, the reconstruction of the Wigner function around the origin of phase space is the least disturbed, but with higher displacements the fluctuations grow stronger as seen in Fig. 4.4. Therefore, it may be beneficial to probe the Wigner function around the origin densely, and sparsely at the higher displacements, in particular $|\alpha| > 1$. Note that probing near the origin doesn't undermine the quality of reconstruction as long as we probe the Wigner function at $2m_0 + 1$ distinct points because we need only $2m_0 + 1$ distinct points to reconstruct a polynomial of degree $2m_0$ as seen in Fig. 4.3.

In fact, we can further exploit the rotational symmetry of the POVMs corresponding to phase insensitive detector, which means the Wigner function at α has the same value at $-\alpha$. This allows us to only probe the Wigner function at $m_0 + 1$ distinct points to fully characterize a quantum detector that saturates at the photon-number m_0. However, in this work we numerically probe the phase space at equidistant displacement amplitudes.

We now investigate how sensitive our reconstruction is to the choice of γ. To evaluate that, we calculate the relative error defined in Eq. (4.25) for several values of $\gamma \in [10^{-4}, 0.012]$. The result is illustrated on the bottom right in Fig. 4.4 for the POVM element corresponding to $n = 1$ and $\eta = 0.90$. We can clearly see that even if we vary γ by an order of magnitude (from 10^{-3} to 10^{-2}), the relative error only changes by less than one percent. This shows that there is sufficient freedom in the choice of γ.

4.6 Summary

We have developed a method for characterizing photodetectors by experimentally obtaining the Wigner functions corresponding to the POVMs describing the detector measurements. The proposed experimental scheme is simple and easily accessible, in particular, for a phase insensitive detector. Augmented with quadratic convex optimization and robust nonlinear fitting techniques, we demonstrated its robustness to the experimental fluctuations.

Future work on this method may involve an account for mode mismatch between the local oscillator and the optical mode of thermal states. This direction of research is motivated by the fact that unlike in the balanced homodyne technique, mode mismatch cannot simply be treated as losses in this method.

Chapter 5
Conclusions

In this dissertation we have examined methods to characterize quantum processes and detectors.

In Chapter 1, I presented a brief survey of the history of the study of light. After introducing the reader to quantum mechanics, I ended this chapter by demonstrating how light is quantized.

In Chapter 2, I introduced the necessary tools used in this dissertation. After defining quadrature operators and Wigner functions, I surveyed various states of light as well as optical processes and detectors. I then presented the formalism of Gaussian quantum information that eases the manipulation of Gaussian states and processes. Finally, I briefly showed the advantage of quantum light in phase estimation.

In Chapter 3, I introduced a method to characterize linear and quadratically nonlinear optical systems. This was done by modifying the standard Mach-Zehnder interferometer. I developed a shot noise limited scheme to characterize linear optical systems. I then showed that by using single photons additionally, we can characterize quadratically nonlinear optical systems also. Finally, I showed that no advantage is gained in sensitivity by using squeezed light along with coherent light as probes.

In Chapter 4, I introduced a method to characterize photodetectors by finding the Wigner functions of its POVM elements. After describing the proposed experimental setup, I then showed how this scheme can be used to characterize a photon-number-resolving detector. I then demonstrated that the resource requirement of the scheme can be reduced if we have prior knowledge about the detector. Finally, I used tools from convex quadratic optimization to make the characterization robust against experimental noise.

Appendix A
Final Covariance matrix for Coherent and Squeezed Vacuum

For simplicity in notations we use the following definitions:

$$x \equiv \mathrm{Re}\left(U_{11}\right), \tag{A.1}$$
$$y \equiv \mathrm{Im}\left(U_{11}\right). \tag{A.2}$$

The elements of the final covariance matrix are as follows:

$$\begin{aligned}
V_{11} &= \frac{1}{4}(2e^{r}x(x\cosh(r)+2\sinh(r)\cos(\phi))+(e^{-2r}+1)y^{2}-4e^{-r}y\sinh(r)\sin(\phi)\\
&\quad+\sinh(2r)\cos(2\phi)+\cosh(2r)-2((x^{2}+y^{2})+3), &\text{(A.3)}\\
V_{12}=V_{21} &= \frac{1}{2}(\sin(\phi)\left(2x\sinh^{2}(r)+\sinh(2r)\cos(\phi)\right)\\
&\quad-y\left(x\sinh(2r)+2\sinh^{2}(r)\cos(\phi)\right)), &\text{(A.4)}\\
V_{13}=V_{31} &= \sinh(r)\cosh(r)(x+\cos(\phi))(y+\sin(\phi)), &\text{(A.5)}\\
V_{14}=V_{41} &= \frac{1}{8}(\sinh(2r)(2(x^{2}-y^{2})-2\cos(2\phi))\\
&\quad+4\cosh^{2}(r)((x^{2}+y^{2})-1)-4(x^{2}+y^{2})+4), &\text{(A.6)}\\
V_{22} &= \frac{1}{4}(\cosh(2r)\left(x^{2}+y^{2}\right)-\sinh(r)\cosh(r)\left(2\left(x^{2}-y^{2}\right)\right)\\
&\quad+4e^{-r}x\sinh(r)\cos(\phi)+4e^{r}(-y)\sinh(r)\sin(\phi)-\sinh(2r)\cos(2\phi)\\
&\quad+\cosh(2r)-\left(x^{2}+y^{2}\right)^{2}+3), &\text{(A.7)}\\
V_{23}=V_{32} &= \frac{1}{8}(\sinh(2r)\left(2\left(x^{2}-y^{2}\right)-2\cos(2\phi)\right)\\
&\quad-4\cosh^{2}(r)\left(\left(x^{2}+y^{2}\right)-1\right)+4\left(\left(x^{2}+y^{2}\right)-1\right)), &\text{(A.8)}\\
V_{24}=V_{42} &= \sinh(r)\cosh(r)(\cos(\phi)-x)(y-\sin(\phi)), &\text{(A.9)}\\
V_{33} &= \frac{1}{4}(2e^{-r}x(x\cosh(r)-2\sinh(r)\cos(\phi))+\left(e^{2r}+1\right)y^{2}\\
&\quad+4e^{r}y\sinh(r)\sin(\phi)-\sinh(2r)\cos(2\phi)+\cosh(2r)-2\left(x^{2}+y^{2}\right)+3), &\text{(A.10)}\\
V_{34}=V_{43} &= \frac{1}{2}(y\left(x\sinh(2r)-2\sinh^{2}(r)\cos(\phi)\right)\\
&\quad+\sin(\phi)\left(2x\sinh^{2}(r)-\sinh(2r)\cos(\phi)\right)), &\text{(A.11)}\\
V_{44} &= \frac{1}{4}(\cosh(2r)\left(x^{2}+y^{2}\right)-\cosh(2r)\left(x^{2}+y^{2}\right)+2\sinh(r)\cosh(r)\left(x^{2}-y^{2}\right)\\
&\quad-4e^{r}x\sinh(r)\cos(\phi)+4e^{-r}y\sinh(r)\sin(\phi)+\sinh(2r)\cos(2\phi)+3) &\text{(A.12)}
\end{aligned}$$

Appendix B
Reuse and Permissions

The following work published in a journal by American Physical Society has been used in this dissertation:

Kevin Valson Jacob, Anthony E. Mirasola, Sushovit Adhikari, and Jonathan P. Dowling, Phys. Rev. A **98**, 052327 (2018). Used with permission of the American Physical Society.

The copyright agreement, which includes a clause for using the article in a dissertation, is as follows:

Physical Review Journals

journals.aps.org/copyrightFAQ.html

October 1, 2008

December 2017

APS Copyright Policies and Frequently Asked Questions

As the author of an APS-published article, may I include my article or a portion of my article in my thesis or dissertation?

Yes, the author has the right to use the article or a portion of the article in a thesis or dissertation without requesting permission from APS, provided the bibliographic citation and the APS copyright credit line are given on the appropriate pages.

Further information

Journals published by the American Physical Society can be found at https://journals.aps.org/.

FAQ Version: December 12, 2017

References

[1] Jonathan P. Home, David Hanneke, John D. Jost, Jason M. Amini, Dietrich Leibfried, and David J. Wineland. Complete methods set for scalable ion trap quantum information processing. *Science*, 325(5945):1227–1230, 2009.

[2] Frank Arute et al. Quantum supremacy using a programmable superconducting processor. *Nature*, 574(7779):505–510, 2019.

[3] M. Suhail Zubairy. *A Very Brief History of Light*, page 3–24. Springer, 2016.

[4] Hans-A. Bacher and Timothy C. Ralph. *Quantum Models of Light*, chapter 4, pages 93–137. John Wiley & Sons, Ltd, 2019.

[5] Christopher Gerry and Peter Knight. *Introductory Quantum Optics*. Cambridge University Press, 2004.

[6] E. Wigner. On the quantum correction for thermodynamic equilibrium. *Phys. Rev.*, 40:749–759, Jun 1932.

[7] Anatole Kenfack and Karol yczkowski. Negativity of the wigner function as an indicator of non-classicality. *Journal of Optics B: Quantum and Semiclassical Optics*, 6(10):396–404, aug 2004.

[8] E. C. G. Sudarshan. Equivalence of semiclassical and quantum mechanical descriptions of statistical light beams. *Phys. Rev. Lett.*, 10:277–279, Apr 1963.

[9] Roy J. Glauber. Coherent and incoherent states of the radiation field. *Phys. Rev.*, 131:2766–2788, Sep 1963.

[10] Daniel F. Walls and Gerard J. Milburn. *Quantum optics*. Springer, 2008.

[11] Pieter Kok, W. J. Munro, Kae Nemoto, T. C. Ralph, Jonathan P. Dowling, and G. J. Milburn. Linear optical quantum computing with photonic qubits. *Rev. Mod. Phys.*, 79:135–174, Jan 2007.

[12] Michael Reck, Anton Zeilinger, Herbert J. Bernstein, and Philip Bertani. Experimental realization of any discrete unitary operator. *Phys. Rev. Lett.*, 73:58–61, Jul 1994.

[13] William R. Clements, Peter C. Humphreys, Benjamin J. Metcalf, W. Steven Kolthammer, and Ian A. Walmsley. Optimal design for universal multiport interferometers. *Optica*, 3(12):1460–1465, Dec 2016.

[14] R. Balian and E. Brezin. Nonunitary bogoliubov transformations and extension of wick's theorem. *Il Nuovo Cimento B Series 10*, 64(1):37–55, 1969.

[15] Sebastian Wüster. *Classical and Quantum field theories of Bose-Einstein condensates*. PhD thesis, Faculty of Science, Department of Physics and The Australian National University, 2007.

[16] Rafal Demkowicz-Dobrzański, Marcin Jarzyna, and Jan Kołodyński. Chapter four - quantum limits in optical interferometry. volume 60 of *Progress in Optics*, pages 345 – 435. Elsevier, 2015.

[17] Michael A. Nielsen and Isaac L. Chuang. *Quantum Computation and Quantum Information: 10th Anniversary Edition*. Cambridge University Press, 2010.

[18] J. F. Poyatos, J. I. Cirac, and P. Zoller. Complete characterization of a quantum process: The two-bit quantum gate. *Phys. Rev. Lett.*, 78:390–393, Jan 1997.

[19] Isaac L. Chuang and M. A. Nielsen. Prescription for experimental determination of the dynamics of a quantum black box. *Journal of Modern Optics*, 44(11-12):2455–2467, 1997.

[20] J. B. Altepeter, D. Branning, E. Jeffrey, T. C. Wei, P. G. Kwiat, R. T. Thew, J. L. O'Brien, M. A. Nielsen, and A. G. White. Ancilla-assisted quantum process tomography. *Phys. Rev. Lett.*, 90:193601, May 2003.

[21] Debbie W. Leung. Choi's proof as a recipe for quantum process tomography. *Journal of Mathematical Physics*, 44(2):528–533, 2003.

[22] M. Mohseni and D. A. Lidar. Direct characterization of quantum dynamics. *Phys. Rev. Lett.*, 97:170501, Oct 2006.

[23] M. Mohseni and D. A. Lidar. Direct characterization of quantum dynamics: General theory. *Phys. Rev. A*, 75:062331, Jun 2007.

[24] A. Shabani, R. L. Kosut, M. Mohseni, H. Rabitz, M. A. Broome, M. P. Almeida, A. Fedrizzi, and A. G. White. Efficient measurement of quantum dynamics via compressive sensing. *Phys. Rev. Lett.*, 106:100401, Mar 2011.

[25] M. Mohseni, A. T. Rezakhani, and D. A. Lidar. Quantum-process tomography: Resource analysis of different strategies. *Phys. Rev. A*, 77:032322, Mar 2008.

[26] Mirko Lobino, Dmitry Korystov, Connor Kupchak, Eden Figueroa, Barry C. Sanders, and A. I. Lvovsky. Complete characterization of quantum-optical processes. *Science*, 322(5901):563–566, 2008.

[27] Aamir Anis and A I Lvovsky. Maximum-likelihood coherent-state quantum process tomography. *New Journal of Physics*, 14(10):105021, oct 2012.

[28] Ilya A Fedorov, Aleksey K Fedorov, Yury V Kurochkin, and A I Lvovsky. Tomography of a multimode quantum black box. *New Journal of Physics*, 17(4):043063, Apr 2015.

[29] M. Ghalaii and A. T. Rezakhani. Scheme for coherent-state quantum process tomography via normally-ordered moments. *Phys. Rev. A*, 95:032336, Mar 2017.

[30] Vittorio Giovannetti, Seth Lloyd, and Lorenzo Maccone. Quantum metrology. *Phys. Rev. Lett.*, 96:010401, Jan 2006.

[31] Pieter Kok, W. J. Munro, Kae Nemoto, T. C. Ralph, Jonathan P. Dowling, and G. J. Milburn. Linear optical quantum computing with photonic qubits. *Rev. Mod. Phys.*, 79:135–174, Jan 2007.

[32] Scott Aaronson and Alex Arkhipov. The computational complexity of linear optics. In *Proceedings of the Forty-third Annual ACM Symposium on Theory of Computing*, STOC '11, pages 333–342, New York, NY, USA, 2011. ACM.

[33] Anthony Laing and Jeremy L. O'Brien. Super-stable tomography of any linear optical device, 2012.

[34] Ish Dhand, Abdullah Khalid, He Lu, and Barry C Sanders. Accurate and precise characterization of linear optical interferometers. *Journal of Optics*, 18(3):035204, Feb 2016.

[35] Saleh Rahimi-Keshari, Matthew A. Broome, Robert Fickler, Alessandro Fedrizzi, Timothy C. Ralph, and Andrew G. White. Direct characterization of linear-optical networks. *Opt. Express*, 21(11):13450–13458, Jun 2013.

[36] Max Tillmann, Christian Schmidt, and Philip Walther. On unitary reconstruction of linear optical networks. *Journal of Optics*, 18(11):114002, 2016.

[37] Nicolò Spagnolo, Enrico Maiorino, Chiara Vitelli, Marco Bentivegna, Andrea Crespi, Roberta Ramponi, Paolo Mataloni, Roberto Osellame, and Fabio Sciarrino. Learning an unknown transformation via a genetic approach. *Scientific Reports*, 7(1), 2017.

[38] Horace P. Yuen. Two-photon coherent states of the radiation field. *Phys. Rev. A*, 13:2226–2243, Jun 1976.

[39] Yanhua Shih. Entangled biphoton source - property and preparation. *Reports on Progress in Physics*, 66(6):1009–1044, May 2003.

[40] Alexander I. Lvovsky. *Photonics Volume 1: Fundamentals of photonics and physics*, pages 121–164. Wiley, West Sussex, United Kingdom, 2015.

[41] Christian Weedbrook, Stefano Pirandola, Raúl García-Patrón, Nicolas J. Cerf, Timothy C. Ralph, Jeffrey H. Shapiro, and Seth Lloyd. Gaussian quantum information. *Rev. Mod. Phys.*, 84:621–669, May 2012.

[42] Gerardo Adesso, Sammy Ragy, and Antony R. Lee. Continuous variable quantum information: Gaussian states and beyond. *Open Systems & Information Dynamics*, 21:1440001, Dec 2014.

[43] Xiang-Bin Wang, Zong-Wen Yu, Jia-Zhong Hu, Adam Miranowicz, and Franco Nori. Efficient tomography of quantum-optical gaussian processes probed with a few coherent states. *Phys. Rev. A*, 88:022101, Aug 2013.

[44] J. Řeháček, S. Olivares, D. Mogilevtsev, Z. Hradil, M. G. A. Paris, S. Fornaro, V. D'Auria, A. Porzio, and S. Solimeno. Effective method to estimate multidimensional gaussian states. *Phys. Rev. A*, 79:032111, Mar 2009.

[45] M. D. Eisaman, J. Fan, A. Migdall, and S. V. Polyakov. Invited review article: Single-photon sources and detectors. *Review of Scientific Instruments*, 82(7):071101, 2011.

[46] Masahiro Takeoka, Kaushik P. Seshadreesan, Chenglong You, Shuro Izumi, and Jonathan P. Dowling. Fundamental precision limit of a mach-zehnder interferometric sensor when one of the inputs is the vacuum. *Phys. Rev. A*, 96:052118, Nov 2017.

[47] Robert H. Hadfield. Single-photon detectors for optical quantum information applications. *Nature Photonics*, 3(12):696–705, 2009.

[48] Christine Silberhorn. Detecting quantum light. *Contemporary Physics*, 48(3):143–156, 2007.

[49] Y. Wang, Z. Wang, Q. Yu, X. Xie, T. Posavitz, M. Jacob-Mitos, A. Ramaswamy, E. J. Norberg, G. A. Fish, and A. Beling. High-power photodiodes with 65 ghz bandwidth heterogeneously integrated onto silicon-on-insulator nano-waveguides. *IEEE Journal of Selected Topics in Quantum Electronics*, 24(2):1–6, March 2018.

[50] Marco Ramilli, Alessia Allevi, Valery Chmill, Maria Bondani, Massimo Caccia, and Alessandra Andreoni. Photon-number statistics with silicon photomultipliers. *J. Opt. Soc. Am. B*, 27(5):852–862, May 2010.

[51] Francesco Mattioli, Zili Zhou, Alessandro Gaggero, Rosalinda Gaudio, Saeedeh Jahanmirinejad, Döndü Sahin, Francesco Marsili, Roberto Leoni, and Andrea Fiore. Photon-number-resolving superconducting nanowire detectors. *Superconductor Science and Technology*, 28(10):104001, 2015.

[52] Danna Rosenberg, Adriana E. Lita, Aaron J. Miller, and Sae Woo Nam. Noise-free high-efficiency photon-number-resolving detectors. *Phys. Rev. A*, 71:061803, Jun 2005.

[53] Mario Krenn, Mehul Malik, Thomas Scheidl, Rupert Ursin, and Anton Zeilinger. *Quantum Communication with Photons*, pages 455–482. Springer International Publishing, Cham, 2016.

[54] Nicolas Brunner, Daniel Cavalcanti, Stefano Pironio, Valerio Scarani, and Stephanie Wehner. Bell nonlocality. *Rev. Mod. Phys.*, 86:419–478, Apr 2014.

[55] J. S. Lundeen, A. Feito, H. Coldenstrodt-Ronge, K. L. Pregnell, Ch. Silberhorn, T. C. Ralph, J. Eisert, M. B. Plenio, and I. A. Walmsley. Tomography of quantum detectors. *Nat. Phys.*, 5(1):27–30, 01 2009.

[56] F. T. Arecchi. Measurement of the statistical distribution of gaussian and laser sources. *Phys. Rev. Lett.*, 15:912–916, Dec 1965.

[57] J.r. Johansson, P.d. Nation, and Franco Nori. Qutip 2: A python framework for the dynamics of open quantum systems. *Computer Physics Communications*, 184(4):1234–1240, 2013.

[58] Mariano Gasca and Thomas Sauer. Polynomial interpolation in several variables. *Advances in Computational Mathematics*, 12(4):377, Mar 2000.

[59] V A Il'in. Tikhonov's work on methods of solving ill-posed problems. *Russian Mathematical Surveys*, 22(2):142–149, apr 1967.

[60] Steven Diamond and Stephen Boyd. CVXPY: A Python-embedded modeling language for convex optimization. *Journal of Machine Learning Research*, 17(83):1–5, 2016.

[61] Bill Triggs, Philip F. McLauchlan, Richard I. Hartley, and Andrew W. Fitzgibbon. Bundle adjustment — a modern synthesis. In Bill Triggs, Andrew Zisserman, and Richard Szeliski, editors, *Vision Algorithms: Theory and Practice*, pages 298–372, Berlin, Heidelberg, 2000. Springer Berlin Heidelberg.

Vita

Kevin hails from the state of Kerala, India where he was born to Suja and Jacob Valson. After attending school in Kerala, in 2010 he moved to Kanpur in north India to learn physics. In 2015, he earned a 5-year Integrated M.Sc. in Physics from Indian Institute of Technology Kanpur. Subsequently, he joined Louisiana State University to pursue his doctoral studies at the Quantum Science and Technology group with Prof. Jonathan Dowling as his advisor. During his PhD he has investigated various aspects of quantum information such as quantum process tomography and quantum detector tomography, as well as using techniques from quantum information to solve problems in quantum chemistry. He plans to receive his Ph.D. in May 2020. He is married to Anu. In his spare time, he enjoys cooking, & playing chess and carrom.